






ORIGINAL RESEARCH

Dynamic *in vivo* monitoring of granum structural changes of *Ctenanthe setosa* (Roscoe) Eichler during drought stress and subsequent recovery

Richard Hembrom¹  | Renáta Ünnepe²  | Éva Sárvári³  | Gergely Nagy⁴  | Katalin Solymosi¹ 

¹Department of Plant Anatomy, Institute of Biology, Faculty of Science, ELTE Eötvös Loránd University, Budapest, Hungary

²Neutron Spectroscopy Department, HUN-REN Centre for Energy Research, Budapest, Hungary

³Department of Plant Physiology and Molecular Plant Biology, Institute of Biology, Faculty of Science, ELTE Eötvös Loránd University, Budapest, Hungary

⁴Neutron Scattering Division, Oak Ridge National Laboratory, Oak Ridge, Tennessee, USA

Correspondence

Katalin Solymosi,
Email: katalin.solymosi@ttk.elte.hu

Gergely Nagy,
Email: nagy@ornl.gov

Funding information

Nemzeti Kutatási, Fejlesztési és Innovációs Alap, Grant/Award Number: ÚNKP-23-5 to K.S.; Tempus Közalapítvány, Grant/Award Number: Stipendium Hungaricum to R.H.; National Research, Development and Innovation Office, Grant/Award Numbers: OTKA FK124748, OTKA PD 138540

Edited by A. Krieger-Liszakay

Abstract

Investigating the effects of drought stress and subsequent recovery on the structure and function of chloroplasts is essential to understanding how plants adapt to environmental stressors. We investigated *Ctenanthe setosa* (Roscoe) Eichler, an ornamental plant that can tolerate prolonged drought periods (40 and 49 days of water withdrawal). Conventional biochemical, biophysical, physiological and (ultra)structural methods combined for the first time in a higher plant with *in vivo* small-angle neutron scattering (SANS) were used to characterize the alterations induced by drought stress and subsequent recovery. Upon drought stress, no significant changes occurred in the chloroplast ultrastructure, chlorophyll content, 77K fluorescence emission spectra and maximal quantum efficiency of PSII (Qy dark), but the actual quantum efficiency of PSII (Qy light) decreased, the amounts of PSI-LHCII complexes and PSII monomers declined, and that of PSII supercomplexes increased. Thickness of the leaf and of the adaxial hypodermis, chloroplast length and granum repeat distance (RD) values decreased upon drought stress, as shown by light microscopy and SANS, respectively. Because of the very slight (nm-range) changes in RD values, the large biological variability (significant differences in RD values among the leaves and studied leaf regions) and the invasive sampling required for this method, transmission electron microscopy (TEM) hardly showed significant differences. On the other side, *in situ* SANS analyses provided a unique insight *in vivo* into the fast structural recovery of the granum structure of drought-stressed leaves, which happened already 18 h after re-watering, while functional and biochemical recovery took place on a longer time scale.

1 | INTRODUCTION

Plants respond to drought stress differently, depending on their habitat, the length and severity of the water unavailability as well as the plant species and development stage (Osakabe et al., 2014; Basu

et al., 2016). Since their radiation onto land during evolution, different plant species have developed various tolerance mechanisms towards water deficit in their environments. Drought tolerance occurs at all levels of organization, starting from the anatomical and morphological levels to physiological, cellular, biochemical, and molecular levels.

This is an open access article under the terms of the [Creative Commons Attribution-NonCommercial-NoDerivs](https://creativecommons.org/licenses/by-nc-nd/4.0/) License, which permits use and distribution in any medium, provided the original work is properly cited, the use is non-commercial and no modifications or adaptations are made.

© 2025 Oak Ridge National Laboratory, managed by UT- Battelle, LLC and The Author(s). *Physiologia Plantarum* published by John Wiley & Sons Ltd on behalf of Scandinavian Plant Physiology Society.

Recently, the significance of the environment-dependent control of thylakoid macrostructure also came into prominence (Kirchhoff, 2019; Johnson & Wientjes, 2020; Rantala et al., 2020; Li et al., 2020; Gu et al., 2022). Lower plants and a few angiosperm species evolved desiccation tolerance mechanisms and can thus survive vegetative desiccation of their tissues (Toldi et al., 2009). Most other flowering plants either rely on the survival of their desiccation-tolerant seeds or try to minimize water loss of their vegetative tissues by either various xeromorphic anatomical features or by increased water storage by succulence. However, drought stress negatively affects the productivity and yield of most crops, often even leading to plant death (Kebbas et al., 2015), and thus represents a global challenge for agriculture and sustainable food production. Therefore, an improved understanding of the plants' drought response mechanisms would be useful for producing resilient crop varieties.

In this work, we chose the evergreen perennial plant *Ctenanthe setosa* (Roscoe) Eichler, commonly known as 'never never plant' or 'prayer plant'. Although native to Brazil, it is also present in certain parts of Central America, such as the rainforest habitats of Costa Rica. The genus of this monocotyledonous flowering plant belongs to the Marantaceae family. It is grown as an ornamental crop and houseplant for its attractive dark green foliage. The plant is spreading horizontally from its rhizome under ideal growth conditions. According to studies (Saglam et al., 2008) the plant can survive up to 60 days without water, which makes it a suitable model plant for studying extreme drought tolerance and subsequent recovery mechanism during long periods of water-withholding followed by re-watering. At the anatomical level, leaf rolling occurs in *C. setosa*, which reduces leaf surface area and transpiration, and thus represents an effective drought avoidance mechanism in plants growing in dry areas and helps to protect the leaves from photodamage (Terzi & Kadioglu, 2006; Kutlu et al., 2009). Light microscopic investigations of the leaves revealed the presence of large hypodermal cells (Kutlu et al., 2009), which is an anatomical trait related to leaf water storage and, thus, succulence in this species.

At the physiological level, drought stress generally has a strong inhibitory effect on photosynthetic activity due to various reasons, including decreased leaf surface area, increased leaf temperature, impaired photosynthetic machinery, and premature leaf senescence (Farooq et al., 2009; Bhargava & Sawant, 2013). Stomatal closure in response to drought stress can be effective in water withholding but also results in a decrease in the photosynthetic rate as was reported in bean (*Phaseolus vulgaris*) (Zlatev & Lidon, 2012) or *Jatropha curcas* (Sapeta et al., 2013). Stomatal guard cell size was shown to decrease in certain phases of drought stress-induced leaf rolling in *C. setosa*, and the stomata appeared closed (Kutlu et al., 2009). According to Giardi et al. (1996) long-term drought stress decreased the photochemical efficiency of photosystem II (PSII) in pea (*Pisum sativum*), also evidenced by a lower quantum yield of PSII (Φ PSII) and larger non-photochemical quenching (NPQ) values in *C. setosa*, whilst other studies showed no significant variations in Φ PSII with increased NPQ until 35 days of drought treatment but a decline later (56 days) (Nar et al., 2009). Inhibition of photosynthesis during drought stress also causes oxidative stress due to the generation of reactive oxygen species (ROS), which affects plant growth and crop yield. In *C. setosa*, drought tolerance is closely associated with the antioxidant enzyme system (Terzi & Kadioglu, 2006),

and an increased amount of superoxide dismutase (SOD), peroxidase, and glutathione reductase (GR) scavenge ROS produced in the symplast and apoplast during drought (Saruhan et al., 2010; Terzi et al., 2013).

The drought-induced dehydration constitutes direct osmotic stress affecting cellular processes. Plants often alter their metabolism in various ways to cope with dehydration stress, including the increased production of osmoregulatory compounds. To withstand osmotic stress, *C. setosa* synthesizes and accumulates phenols, fructose, glucose, inositol, and sucrose predominantly in the cytoplasm and other plant organelles, thereby maintaining turgor pressure and cell water homeostasis during the drought period (Nuccio et al., 1999; Saglam et al., 2014).

Cellular responses to drought stress in *C. setosa* also include modification of the cell cycle and cell division, changes in the lipids and fatty acids (Ayaz et al., 2001), endomembrane system and vacuolization of cells, and alterations in cell wall architecture (Terzi et al., 2013). However, to the best of our knowledge, no ultrastructural data are available about *C. setosa*, and about how, for instance, drought stress and subsequent recovery affect its chloroplast ultrastructure. Overall, literature data about how drought stress affects plastid ultrastructure in other species is also controversial. Some studies report the somewhat counterintuitive swelling of the intrathylakoidal space called lumen in chloroplasts of drought-stressed plants (Zhang et al., 2015; Bai et al., 2016; Shao et al., 2016), while others do not observe similar alterations in plastid structure (Chen et al., 2018).

In this paper, we investigated the chloroplast ultrastructure of *C. setosa* in parallel to its photosynthetic characteristics after long-term drought stress and during rehydration-induced recovery. As sample preparation of drought-stressed samples for TEM involves a first step of fixation in a water-based solution, which may alter the drought-stressed status and may result in fixation artefacts, it is crucial to validate the ultrastructural data obtained by conventional transmission electron microscopy (TEM) with non-invasive, *in vivo* measurements such as small-angle neutron scattering (SANS) (Ünnep et al., 2014a; Ünnep et al., 2020; Ounoki et al., 2021). The latter method has been proven to provide insight into spatially averaged dynamic changes and reorganization of chloroplast inner membranes of various organisms (Nagy & Garab, 2021). On the other side, with very few exceptions (e.g., Ounoki et al., 2021), most of the SANS studies on flowering plants have been performed on excised and often D₂O infiltrated leaves or leaf segments, thus not in fully intact plants under physiologically and environmentally relevant, entirely natural conditions. Ounoki et al. (2021) studied intact rooted spearmint plants grown in hydroponic culture, not in soil. Therefore, in this study, we also wanted to explore the potential of SANS to monitor granum structural changes during drought stress and subsequent structural recovery *in vivo* in potted plants.

2 | MATERIALS AND METHODS

2.1 | Plant material and treatments

Adult *Ctenanthe setosa* (Roscoe) Eichler 'Grey Star' plants were purchased and delivered from California Tropicals LLC (Irvine, CA, USA) during summer (for the SANS measurements performed in the USA), or were obtained from the ELTE Botanical Garden, Budapest,

Hungary throughout the year (for all other measurements). The plants were then acclimatized to the lab environment for a week under the following conditions: natural light of 100–150 $\mu\text{mol photons s}^{-1}\text{m}^{-2}$ photon flux density, 12:12h photoperiod, while the humidity varied from 25 to 30%. The room temperature ranged between 22°C and 26°C. The plants were continuously grown under well-watered conditions (Control, ‘Ctrl’ in the Figures) or were subjected to drought stress for a period of 40–49 days followed by re-watering for 21–28 days. Leaves were sampled from the drought-stressed plants (‘Dry’) and after their re-watering, i.e. during recovery for 1 day (‘R-1d’), 7 days (‘R-7d’), 21 days (‘R-21d’) and 28 days (‘R-28d’). Fully developed leaves of continuously well-watered adult plants of the same clone and plant size as those used for drought stress were also measured as control. Control leaves collected from control plants simultaneously with the ‘Dry’ leaves of drought-stressed plants (i.e. 40–49 days after the beginning of the experiment) will be referred to as control leaves (‘Ctrl’), while control leaves collected 28 days later (i.e., at the same time as ‘R-28d’ recovered leaves) are designated as ‘Ctrl-R’ leaves.

In the case of SANS experiments, plants were acclimated to ambient light and temperature conditions in the vicinity of the Oak Ridge National Laboratory (ORNL) in September 2021. Each pot contained one plant. Each plant was assigned a number, and each measured leaf was marked in a non-invasive way – using a paper labelling ring – around their petiole, allowing the tracking of the same leaves at different time-points of the measurement. Fully developed, large leaves were chosen for the measurements. Because of their strong dark green color and potentially different plastid structure, we avoided the visible leaf veins and only measured and sampled the interveinal regions.

2.2 | Determination of leaf relative water content

The relative water content (RWC) was determined gravimetrically by weighing leaf discs before (fresh weight) and after maintaining the leaf discs in the dark on wet filter paper under water-saturated conditions for 16 h (saturated weight), followed by oven drying at 80°C to a constant mass (dry weight), using the equation: $\text{RWC (\%)} = 100 \cdot (\text{fresh weight} - \text{dry weight}) / (\text{saturated weight} - \text{dry weight})$. For all treatments, 4–9 independent repetitions were measured.

Similarly, the soil water content (SWC) was calculated as $\text{SWC} = 100 \cdot (\text{fresh weight} - \text{dry weight}) / (\text{saturated weight} - \text{dry weight})$. In this case, fresh weight was determined by measuring soil weight on each day of the drought treatment. For the dry weight measurement, soil was air-dried until a constant weight was achieved. Saturated weight was measured when soil was fully water-saturated.

2.3 | Determination of pigment contents

Pigments were extracted from leaf discs or thylakoids with buffered [5 mM N-(Tri(hydroxymethyl)methyl) glycine (Tricine)-KOH pH 7.8] 80% (v/v) acetone at low light. The extracts were centrifuged at 4°C with 10,000 \times g for 5 min, and absorption spectra (400–800 nm) were

measured spectrophotometrically by a UV-VIS spectrophotometer (UV-1601, Shimadzu). Carotenoid and chlorophyll (Chl) contents were calculated according to Lichtenthaler (1987) and Porra et al. (1989), respectively. For all treatments, 4–6 independent repetitions were measured.

2.4 | 77K fluorescence emission spectra

Stripes from the interveinal region (max. 2 \times 10 mm) were carefully collected, then put into glass tubes and immersed in liquid nitrogen (77K). As the studied *C. setosa* cultivar has anthocyanin-colored purplish abaxial leaf surface, spectra were always recorded from the green adaxial leaf surface. A Fluoromax-3 spectrofluorometer (Horiba Jobin Yvon) was used to record 77K fluorescence emission spectra with 440 nm excitation, 2 and 5 nm excitation and emission slits, respectively. An average of 3 spectra were recorded in all cases. Emission signals were corrected for wavelength-dependent sensitivity of the detection, baseline correction and 3- or 5-point linear smoothing were done using SPSEV V3.14 software (copyright: C. Bagyinka, Institute of Biophysics, HUN-REN Biological Research Centre, Szeged, Hungary). Normally, 5–7 independent repetitions were measured for all treatments. Spectra were normalized to their maxima and then averaged. The relative fluorescence emission maximum values of the major 77K fluorescence bands of the different samples were compared statistically.

2.5 | Thylakoid isolation and 2D Blue Native/ SDS PAGE

Leaves were homogenized in 50 mM 4-(2-hydroxyethyl)-1-piperazineethanesulphonic acid (HEPES)-KOH (pH 7.0), 330 mM sorbitol, 2 mM ethylenediaminetetraacetic acid (EDTA), 2 mM MgCl_2 , 0.1% (w/v) bovine serum albumin (BSA), 0.1% (w/v) Na-ascorbate at 4°C for 2 \times 3 s by Waring blender. The homogenate was filtered through four layers of gauze and two layers of Miracloth™ (Calbiochem-Novabiochem). Chloroplasts were immediately pelleted by centrifugation (1,500 \times g, 5 min, 4°C). The pellet was resuspended in a washing buffer (50 mM HEPES-KOH pH 7.0, 330 mM sorbitol, 2 mM MgCl_2). Osmotic shock and removal of coupling factor 1 (CF₁) was carried out as described previously (Sóti et al., 2023).

Blue Native (BN) and SDS PAGE were done using Mini-Protean apparatus (BioRad) and evaluated according to (Sárvári et al., 2022). Shortly, thylakoids (500 $\mu\text{g Chl ml}^{-1}$) were solubilized using 1% (w/v) n-dodecyl- β -D-maltoside (β -DM) plus 1% (w/v) digitonin. Solubilization of thylakoids was higher than 90% in all cases. Complexes were separated in 4.3–12% BN gel gradient. Polypeptide patterns of complexes were obtained by applying cut BN lanes on the top of 10–18% SDS PAGE gradient containing 8.7% (w/v) glycerol. The gels scanned using an Epson Perfection V750 PRO scanner were densitometrically analyzed using the Phoretix image analysis software (Phoretix International). The isolation of thylakoids was repeated 2–3 times, and 4–6 technical repetitions by 2D BN/SDS PAGE were carried out with all isolated samples.

2.6 | Measurement of chlorophyll a fluorescence induction

Fast chlorophyll fluorescence induction was measured with a portable instrument (FluorPen FP 100, Photon Systems Instruments) both in light-adapted and 20-min dark-adapted states, by applying saturating light ($2050 \mu\text{mol photons s}^{-1} \text{m}^{-2}$). Values recorded after the application of 1 s saturating light will be referred to as Q_y light and Q_y dark data corresponding to F_V/F_M' and F_V/F_M values, respectively. F_M corresponds to maximal fluorescence intensity after saturating light, F_0 is ground fluorescence ($F_{50\mu\text{s}}$, fluorescence intensity at 50 μs), and F_V refers to maximal variable fluorescence, calculated as $F_M - F_0$ in dark-adapted samples (Q_y dark). The same parameters in light-adapted samples are designated with primes (e.g., F_V' etc.).

After the application of 2 s of saturating light, the rapid fluorescence transient, referred to as the OJIP with the following parameters, was determined according to (Strasser et al., 2000). Parameters related to OJIP transients were recorded as described below in line with the instrument manual. F_J corresponds to fluorescence intensity at J-step (at 2 ms), while F_I is the fluorescence intensity at I-step (at 30 ms). The relative variable fluorescence at 2 ms is calculated as $V_J = (F_J - F_0)/(F_M - F_0)$, the relative variable fluorescence at 30 ms is $V_I = (F_I - F_0)/(F_M - F_0)$, and $\text{Phi}_{Pav} = \text{Phi}_{P_0}(S_M/t_{F_m})$, where $\text{Phi}_{P_0} = 1 - (F_0/F_m)$, S_M is defined as $S_M = \text{Area}/(F_m - F_0)$, where the area is the one between the fluorescence curve and F_M (background subtracted), and t_{F_m} is the time needed to reach F_M (in ms).

Altogether, 20–188 biological replicates were measured from 9 ‘Ctrl’, 14 ‘Dry’ and 2–8 recovered plants in 2–8 independent experiments. Different adaxial leaf regions (base, middle region, and tip region) were measured for each leaf. We observed large biological variability in the data obtained in the leaf tip regions; therefore, our data represent the mean and standard deviation values of the measurements obtained for the leaf base and middle regions only.

2.7 | Light microscopy (LM) and transmission electron microscopy (TEM)

1×1 mm middle region interveinal leaf blade sections of light-acclimated plants were fixed in 2.5% (v/v) glutaraldehyde for at least 3 h, then post-fixed in 1% OsO_4 (w/v) for 2 h, both buffered with 70 mM $\text{Na}_2\text{HPO}_4 - \text{KH}_2\text{PO}_4$ (pH 7.2). After each fixation step, the excess fixatives were washed out by rinsing the samples three times for 15 min with the same buffer. Following dehydration in an ascending ethanol series, samples were embedded in Durcupan ACM resin (Fluka).

Semi-thin sections (1 μm) or ultrathin sections (70 nm) were prepared on a Reichert Jung ultramicrotome for LM and TEM, respectively. After toluidine blue staining, the semi-thin sections were observed with an Olympus BH2-RFCA light microscope. Light micrographs were recorded using a Nikon COOLPIX 950 digital camera. Measurements of leaf thickness (on at least 3–4 different sections) and chloroplast dimensions (on $n=22$ –153 plastids) were performed on light micrographs using ImageJ software as described in Adolfsson et al. (2015).

Ultrathin sections mounted on copper grids were contrasted with uranyl acetate and lead citrate before being analyzed by a JEOL JEM 1011 TEM. ImageJ software was used to determine ultrastructural quantitative parameters (repeat distance values) as in Ünneper et al. (2014b) on randomly chosen grana ($n=88$ –182) from 29–85 plastid sections taken randomly from mesophyll cells located in the interveinal region of the middle of the leaf blade. Three different control leaves (from three different control plants), two different leaves from a 45-day drought-stressed plant, as well as two different leaf regions of a 49-day drought-stressed plant were analyzed and compared to provide information about the biological variability of the data.

2.8 | Small-angle neutron scattering

SANS experiments were performed at the Extended Q-Range Small-Angle Neutron Scattering Diffractometer (EQ-SANS) at the Spallation Neutron Source (SNS) of the Oak Ridge National Laboratory (ORNL) (Heller et al., 2018). Some preliminary experiments were done at the ‘Yellow Submarine’ instrument (Budapest Neutron Center) (Füzi et al., 2017; Almásy, 2021), with experimental settings described in the Supporting Information (Methods S1). Plants, together with the soil and pots, were placed in the sample environment area. Interveinal middle regions of individual leaves were fixed to the end of the collimation section of the beamline to ensure the use of the entire neutron beam. To increase scattering and reduce the required measurement times, rolled-up (dry state) leaves were measured without flattening and flat leaves were gently bent in half along their midrib. Avoiding the flattening of dry rolled-up leaves also reduced the probability of leaf damage. Leaves were measured under ambient temperature and humidity conditions similarly to other experiments.

Two instrument configurations were used: the 30 Hz – so-called – frame-skipping mode using 4 m sample-to-detector distance with the 0.25–0.614 nm and 0.978–1.342 nm wavelength bands offering a cumulative momentum transfer ($Q = 4\pi \frac{\sin\theta}{\lambda}$, where 2θ is the scattering angle and λ is the wavelength of the neutron) coverage of 0.045–4.5 nm^{-1} , and the 60 Hz mode using 4 m sample-to-detector distance with 0.6–0.964 nm wavelength band offering a momentum transfer coverage of 0.06–1.95 nm^{-1} . Due to the wider momentum transfer coverage, analysis of the scattering results was primarily performed on data collected with the 30 Hz operation mode.

Data reduction was performed with the help of the recently developed drtsans software (Heller et al., 2022), Mantid Workbench (Arnold et al., 2014) and Jupyter Notebooks (Kluyver et al., 2016). Scattering intensities were corrected for detector sensitivity, background (air) scattering and transmission values. The data obtained were azimuthally averaged. Due to the variable thickness of the leaves and the varying number of layers in the beam, the data is not presented on an absolute scale.

To facilitate the comparison of scattering curves from different leaves or from different plants, all scattering curves are normalized to 1 at $q \approx 0.1 \text{ nm}^{-1}$, which is below the characteristic diffraction features of our primary interest.

The obtained azimuthally averaged scattering intensities were fitted with a sum of multiple power-law functions and peak functions. In detail, the fitting function can be described as:

$$I(q) = Bg + \sum_{i=1}^3 A_i * q^{p_i} + \sum_{i=1,3 \text{ or } i=1,3,4} \frac{B_i}{w_i \sqrt{\frac{\pi}{2}}} e^{-\frac{2(q-q_{c2})^2}{w_i^2}} + \frac{B_2}{w_2 \sqrt{\frac{\pi}{2}}} e^{-\frac{2(q-q_{c2})^2}{w_2^2}} * \left(\frac{1}{2} + \frac{1}{2} * \text{erf} \left(\frac{sk_2 * (q - q_{c2})}{\frac{w_2}{\sqrt{2}}} \right) \right)$$

The power-law components can be attributed to scattering from the various cellular materials in the complex leaf sample. The prominent peak visible at c.a. 0.3 nm^{-1} was earlier proven to originate from the periodic structure of the granum thylakoid membranes (Ünneper et al., 2014b). The exceptional wavelength resolution of the EQ-SANS instrument allowed the observation of an asymmetric nature of this peak, which is captured in the skewed normal distribution component of the fitting function. Additional 2 (in the case of all the wet and part of the dry leaves) or 3 (in the case of the more excessively dry leaves) Gaussian peaks allowed to well approximate the SANS scattering curves in the entire measured momentum transfer range.

An example of the fitting results can be seen in Figure S1.

The RD of the thylakoid membranes was calculated according to the equation $RD = \frac{2\pi}{q_{c2_mean}}$, where q_{c2_mean} is the mean of the skewed normal distribution. For details about the calculation of the mean of the distribution, see the Supporting Information (Methods S2).

2.9 | Statistical analysis

GraphPad Prism 9 software (USA) was used for statistical analyses. In case of samples showing normal distribution, ordinary one-way ANOVA, followed by Tukey-Kramer multiple comparisons test were performed. In other cases, Kruskal-Wallis test followed by Dunn's multiple comparisons test were performed. For data about percentage and amount values of protein complexes (Figures 3 and S3) the average values and standard deviations were compared using Brown-Forsythe and Welch ANOVA, followed by Dunnett's T3 multiple comparison test. In case of RD values obtained by SANS and TEM, control and dry samples were compared using Welch's test. Differences were considered significant at $P \leq 0.05$.

3 | RESULTS

3.1 | Leaf anatomy under drought stress

C. setosa plants are extremely drought tolerant and can survive without any watering for 40–49 days; however, leaf rolling occurs in the drought-stressed stage (Figure 1). Light microscopic analyses revealed that *C. setosa* has dorsiventral leaves with heterogenous mesophyll being divided into elongated adaxial palisade parenchyma and abaxial spongy

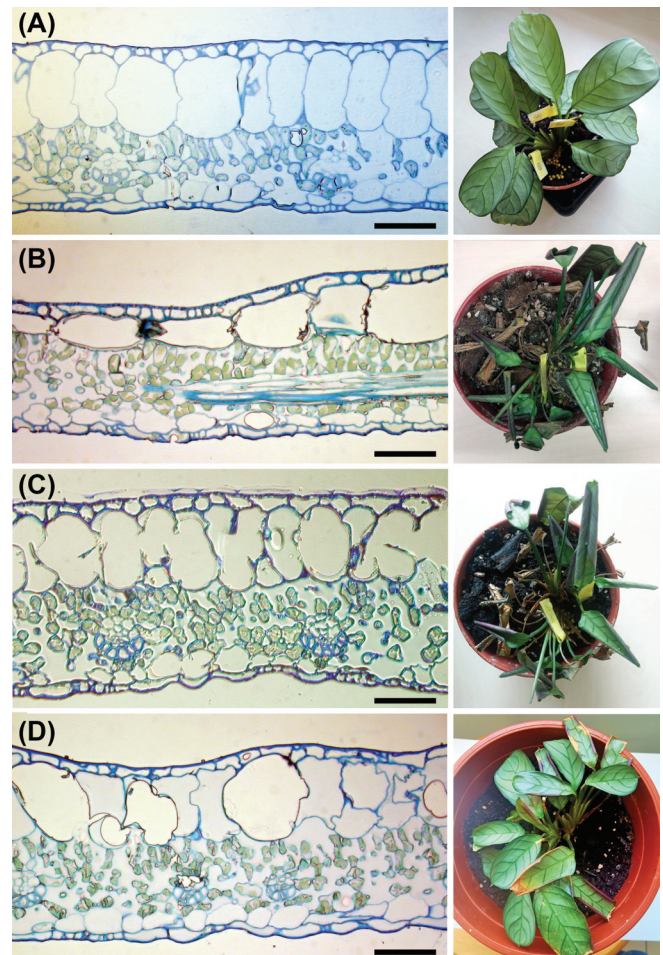


FIGURE 1 Light micrographs and photos of *C. setosa* leaves during the experiments. (A) Control, well-watered plant; (B) 49-day drought-stressed plant; (C–D) plant recovered for 18 h (C) and 21 days (D) after drought stress, respectively. Scale bar: $50 \mu\text{m}$.

parenchyma cells (Figure 1). Below the epidermis, we observed huge hypodermal cells at the adaxial side, while smaller but still prominent hypodermal cells were located below the abaxial epidermis. Similar large hypodermal cell layers are often associated with water storage in succulent plants (Griffiths & Males, 2017). The small mesophyll cells seemed to harbor few large chloroplasts. After 45–49 days of drought stress, the thickness of the leaves, and especially of the hypodermal cell layer, decreased when compared with those of well-watered, control plants' leaves (Table 1). In the plants that recovered for 21 days after drought stress, leaf thickness was restored (Figure 1). Leaf structure also recovered, especially in the mesophyll regions (Figure 1); however, the infiltration of the adaxial hypodermal cell layer was somewhat hindered upon drought stress and also in samples collected during recovery.

3.2 | Leaf relative water content and pigment composition during stress and subsequent recovery

The RWC of leaves decreased to about 60% of the control value after drying for more than 40 days ('Dry') and was recovered 28 days

TABLE 1 Changes in the various anatomical parameters in the leaves of *C. setosa* plants under different treatments. ‘Ctrl’: control leaf; ‘Dry’: leaves from plants exposed to 40–49 days of drought stress; ‘R-18h’ and ‘R-21d’: leaves of drought-stressed plants sampled after 18 h and 21 days of recovery, respectively; ‘Ctrl-R’ – Ctrl leaf analyzed at the same time as ‘R-21d’. Means and standard error values are shown in μm , and significant differences are indicated by different letters according to ordinary one-way (height of the adaxial epidermis, spongy parenchyma, and entire mesophyll), or Kruskal-Wallis (for the other measured parameters) ANOVA followed by Tukey’s or Dunn’s multiple comparison post hoc tests ($P \leq 0.05$), respectively ($n = 16$ – 19 for tissue layers and $n = 22$ – 153 for chloroplast size).

	Ctrl	Dry	R-18h	R-21d	Ctrl-R
Entire leaf width	173.2 \pm 3.0 ^a	150.0 \pm 4.0 ^{bc}	149.4 \pm 2.0 ^{bc}	158.8 \pm 3.4 ^{ac}	139.4 \pm 2.0 ^b
Adaxial epidermis	11.7 \pm 1.0 ^a	8.5 \pm 7.6 ^b	10.2 \pm 0.6 ^{ab}	10.2 \pm 0.7 ^{ab}	10.2 \pm 0.7 ^{ab}
Adaxial hypodermis	68.0 \pm 2.6 ^a	50.5 \pm 2.0 ^b	63.0 \pm 1.1 ^a	65.7 \pm 2.3 ^a	64.7 \pm 1.5 ^a
Entire mesophyll	64.4 \pm 1.1 ^a	55.6 \pm 1.4 ^{bc}	50.9 \pm 1.4 ^b	59.8 \pm 1.6 ^{ac}	50.6 \pm 1.4 ^b
Palisade parenchyma	40.0 \pm 2.8 ^a	34.4 \pm 2.5 ^{ab}	30.7 \pm 1.9 ^b	35.6 \pm 2.7 ^{ab}	30.8 \pm 2.4 ^b
Spongy parenchyma	29.6 \pm 1.1 ^a	25.7 \pm 1.1 ^{ab}	23.6 \pm 1.1 ^b	28.6 \pm 1.1 ^a	23.7 \pm 1.0 ^b
Abaxial hypodermis	17.3 \pm 1.1 ^a	18.2 \pm 4.7 ^a	12.5 \pm 1.1 ^a	15.0 \pm 1.2 ^a	16.0 \pm 1.4 ^a
Abaxial epidermis	9.9 \pm 0.8 ^a	6.0 \pm 0.5 ^b	6.5 \pm 0.4 ^{ab}	7.0 \pm 0.4 ^{ab}	7.5 \pm 0.6 ^{ab}
Chloroplast length	5.8 \pm 0.1 ^a	5.1 \pm 0.1 ^b	5.7 \pm 0.1 ^a	5.5 \pm 0.1 ^a	5.6 \pm 0.2 ^{ab}
Chloroplast width	2.6 \pm 0.1 ^{ab}	2.6 \pm 0.1 ^a	3.4 \pm 0.1 ^{cd}	3.0 \pm 0.1 ^{bd}	3.1 \pm 0.2 ^{bd}
Chloroplast length/width	2.4 \pm 0.1 ^a	2.1 \pm 0.1 ^{ac}	1.8 \pm 0.1 ^b	1.9 \pm 0.1 ^{bc}	1.9 \pm 0.1 ^{bc}

TABLE 2 Soil and leaf relative water contents (RWC), and pigment composition of the leaves of differently treated *C. setosa* plants. Control plants (‘Ctrl’); plants subjected to 40–49 days of drought stress (‘Dry’); and subsequently recovered plants (‘R-1d’, ‘R-7d’, and ‘R-28d’) were sampled 1 day, 7 days, and 28 days after re-watering, respectively. ‘Ctrl-R’ – Ctrl leaf analyzed at the same time as R-28d. Chl $a+b$ values are provided in mg Chl g^{-1} DW. Chl – chlorophyll, Car – carotenoid. Mean and standard error values, as well as significant differences at $P \leq 0.05$ among treatments are indicated with different letters according to ordinary one-way (RWC, Chl $a+b$ and Chl a/b) or Kruskal-Wallis (Car/Chl) non-parametric ANOVA followed by Tukey’s or Dunn’s multiple comparisons post hoc tests, respectively ($n = 3$ – 21).

	Soil RWC (%)	Leaf RWC (%)	Chl $a+b$ mg g^{-1} DW	Chl a/b	Car/Chl
Ctrl	92.7 \pm 3.2 ^a	97.4 \pm 0.8 ^a	12.5 \pm 0.9 ^a	3.01 \pm 0.04 ^a	0.23 \pm 0.00 ^a
Dry	11.0 \pm 0.8 ^b	59.7 \pm 1.0 ^b	12.3 \pm 0.7 ^a	3.05 \pm 0.11 ^a	0.23 \pm 0.00 ^a
R-1d	89.4 \pm 2.2 ^a	64.4 \pm 1.3 ^b	11.7 \pm 1.4 ^a	3.11 \pm 0.15 ^a	0.22 \pm 0.02 ^a
R-7d	96.7 \pm 1.6 ^a	74.1 \pm 1.3 ^{bc}	12.2 \pm 0.8 ^a	3.08 \pm 0.06 ^a	0.23 \pm 0.01 ^a
R-28d	95.2 \pm 1.0 ^a	95.1 \pm 0.5 ^{ab}	12.8 \pm 0.9 ^a	2.97 \pm 0.03 ^a	0.24 \pm 0.01 ^a
Ctrl-R	95.8 \pm 1.2 ^a	99.0 \pm 1.6 ^{ab}	12.7 \pm 1.5 ^a	2.92 \pm 0.06 ^a	0.24 \pm 0.00 ^a

after re-watering (Table 2). Soil relative water content continuously decreased to approximately 11% by day 45 of the drought period and recovered after 7 days of the re-watering period (Figure S3). The pigment content of leaves did not change significantly during the treatments (Table 2).

3.3 | Organizational changes in the structure of the photosynthetic apparatus

Leaf fluorescence emission spectra of green plants exhibit three major 77K fluorescence peaks at 686, 695, and 730–750 nm (Murata et al., 1966). No significant alterations were detected among the control and the differently treated samples in the fluorescence bands at 686 and 695 nm (Figure 2), linked mostly to the PSII (Kalaji et al., 2017; Yokono et al., 2019). The long-wavelength major emission band (emission from PSI-LHCI) appeared at 748 nm, which is

slightly shifted to the red region of the spectra when compared to green leaves of other species (Bos et al., 2023), but the difference across the samples was not significant. Due to reabsorption effects, the 77K fluorescence emission of the pigments of the leaves is probably skewed towards PSI emission, resulting in the observed low relative fluorescence intensities of the 686 and 695 bands in the spectra.

To further characterize the structural organization of the photosynthetic apparatus, we investigated the Chl-protein pattern of thylakoids. The BN-PAGE separation of *C. setosa* thylakoids resulted in 13 clear bands in addition to megacomplexes and Lhc-m (Figure 3A). They were identified based on their polypeptide patterns as PSI, PSII, LHCII, and Cyt b_6/f complexes in different organization forms (Figure S4).

The complex patterns hardly changed during the treatments (Figure 3A). Regarding the ratio of the main complexes, PSI/PSII was practically unchanged, while LHCII/PSII showed some decrease during

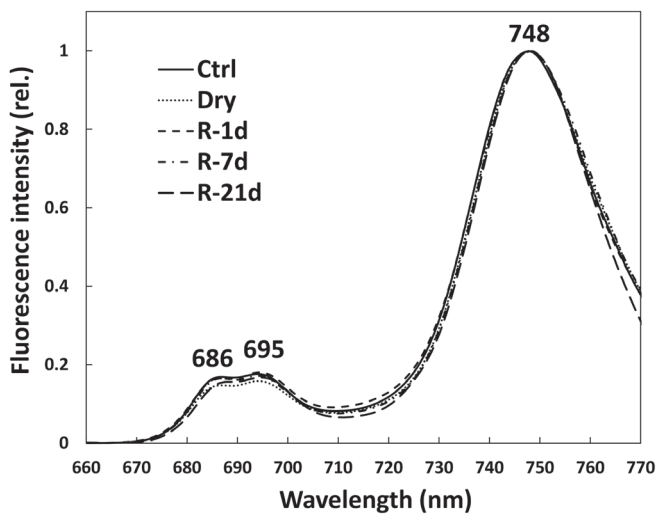


FIGURE 2 77K fluorescence spectra of leaves of control *C. setosa* plants ('Ctrl'); plants exposed to 40-49 days of drought stress ('Dry'); and subsequently recovered plants ('R-1d', 'R-7d', and 'R-21d' were sampled 1 day, 7 days, and 21 days after re-watering, respectively). The figure shows the average of normalized spectra ($n=5-7$) recorded with 440 nm excitation wavelength.

drought stress (Figure 3B). Comparing the organization forms of the different complexes (Figures 3C and S5), a decline of the PSI-LHCII/PSI was observed, and significantly more PSII supercomplexes (PSII-s) and fewer monomers were present in dried plants. Most of the changes were reversed after recovery. Some increase in the trimers (LHCII-t) and monomers (Lhc-m) was found in the thylakoids isolated from the 'Ctrl-R' leaves (Figures 3C and S5).

3.4 | Variations in the physiological characteristics of the leaves

We determined the average Q_y light and Q_y dark values, which characterize the structural dynamics as well as the photochemical activity of PSII (Garab et al., 2023; Sipka et al., 2021) in the light- and dark-adapted samples, respectively (Figure 4). After 40-49 days of drought stress, the Q_y light value in stressed plants declined slightly but significantly; this decline continued on the 1st day of re-watering, recovered after 7 days of re-watering, but slightly declined on 21 days of recovery (Figure 4A). The Q_y dark value remained constant before and after the drought stress treatments (Figure 4B).

In order to further characterize the photosynthetic activity, we have recorded the OJIP curves of the leaves. A slight increase in the O-J-I phases was observed after 40-49 days of drought stress in the OJIP curves, which recovered to shapes like the control only after 21 days of recovery (Figure 5). The analyses of maximum fluorescence (F_M) values without normalization showed significantly

increased fluorescence during the drought period and up to the 7 days of recovery, while they were similar to control values after 21 days of recovery (Table S1). Similarly, significant differences were found in the drought-stressed samples (and during early phases of their recovery) for the other parameters (V_j and V_i) characterizing the OJIP curves, while Φ_{Pav} was significantly different in samples during the recovery stage (Table S1).

3.5 | Analysis of changes in the chloroplast ultrastructure by TEM

Detailed ultrastructural analyses of the middle interveinal regions of the light-adapted leaves by TEM revealed an almost unchanged chloroplast structure with intact chloroplast envelope and inner membrane system during drought stress and the subsequent recovery (Figure 6). No significant differences were observed in the morphology, size and structure of the palisade or spongy parenchyma, and chloroplasts during the treatments (Table 1). Interestingly, we observed chloroplasts with either electron-transparent or electron-dense plastoglobuli both in control and drought-stressed samples from different plants, and plastoglobule size also varied among leaves and treatments (Figure 6), but even within a leaf. In control leaves, starch was present, but it disappeared during drought stress. No visible changes occurred to grana during the drought stress period and the recovery (Figure 6).

The granum RD values of leaf chloroplasts of control, drought-stressed, and recovered *C. setosa* plants were also determined (Table 3). For comparison, we checked the RD values of three different control plants ('Ctrl 1', 'Ctrl 2' and 'Ctrl 3', with only 1 leaf studied for each plant, and typical chloroplasts for the first two samples shown in Figure 6), and two drought-stressed plants: one from a plant drought-stressed for 45 days ('Dry-45 1') and the other for 49 days ('Dry-49 1'). The leaves of the three control plants had significantly different RD values, and we found significant differences even among the different studied leaf regions (next to each other, but still in the middle interveinal region) of the same leaf of the 49-day drought-stressed plant (see data of 'Dry-49, leaf 1, regions 1 and 2') (Table 3). Some significant differences were found in the RD values of the two studied drought-stressed leaves as well. In spite of this large biological variability, Welch's test-based comparison of control and drought-stressed leaves' data indeed showed a significant decrease in RD values under drought stress.

RD values of the grana in the 49-day drought-stressed and then recovered plant's leaves were only significantly lower than those of the 'Ctrl 2' and 'Ctrl 3' plants, and were only significantly higher when compared with the data obtained in one of the 45-day drought-stressed leaves ('Dry-45 1, leaf 1') (Table 3). However, for invasive TEM sampling, we obviously used different leaves from the same plant, which makes our data hard to compare.

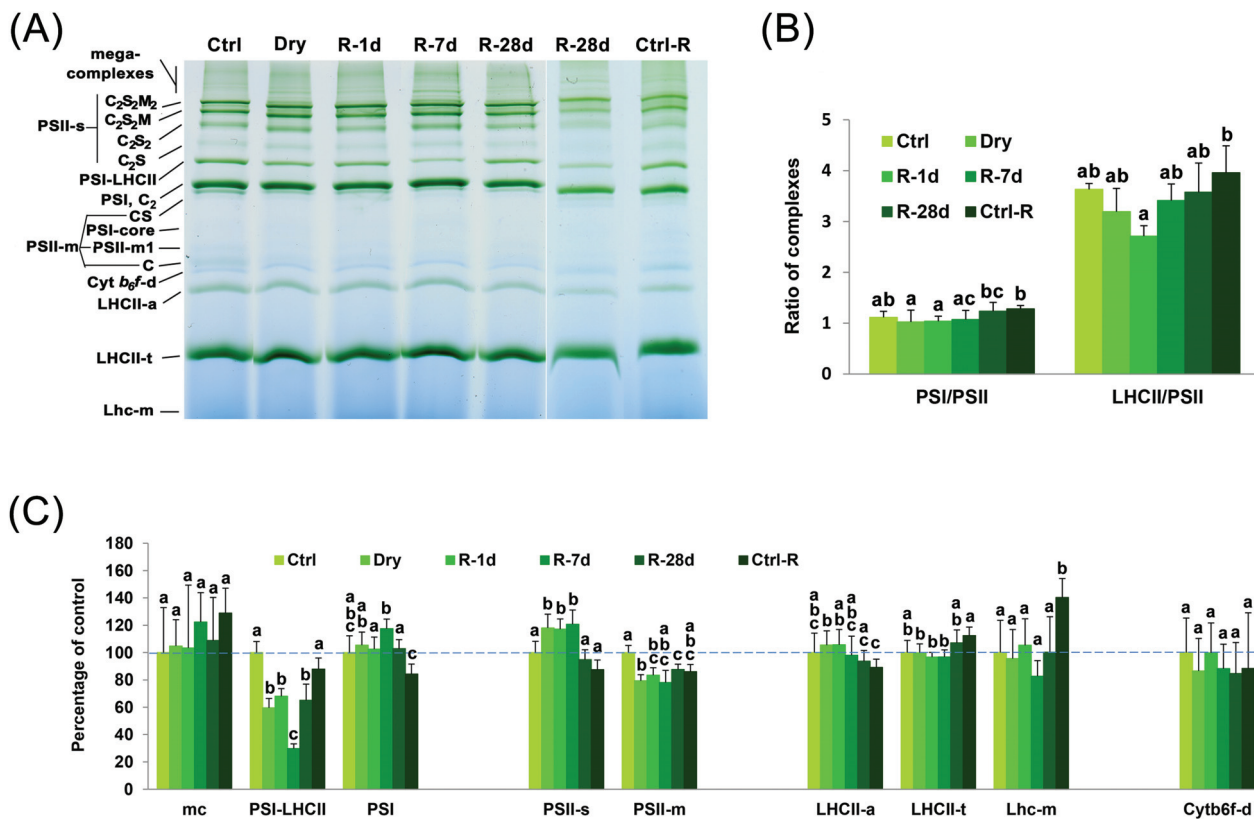


FIGURE 3 Changes in the amounts and ratios of thylakoid complexes in leaves of differently treated *C. setosa* plants. ‘Ctrl’ – thylakoids isolated from control plants at the same time as dry samples; ‘Dry’ – thylakoids isolated from plants exposed to 40–49 days of drought stress; ‘R-1d’, ‘R-7d’, and ‘R-28d’ – thylakoids isolated from recovered plants sampled 1 day, 7 days, and 28 days after re-watering of dry plants, respectively; ‘Ctrl-R’ – Ctrl isolated at the same time as ‘R-28d’. PS – photosystem, C – PSII core, LHC (Lhc) – light-harvesting complex, S, M – strongly, and moderately attached LHCII trimers, PSII-m1 – a little larger complex than PSII-m also containing PSII proteins, LHCII-a – LHCII-assembly: CP29-CP24-LHCII-t, Cyt b₆/f – cytochrome b₆/f complex, s – supercomplex, t – trimer, d – dimer, m – monomer. (A) BN patterns of thylakoid complexes. Thylakoids (500 µg Chl ml⁻¹) were solubilized using 1% β-DM plus 1% digitonin and separated in a 4.3–12% gel gradient. (B) Changes in the ratios of the main complexes. The PSI/PSII ratios were calculated from the pixel densities of the PSI and PSII BN bands (these bands contain the bound antennae), while the LHCII/PSII ratios were calculated from the second dimensional SDS PAGE as the ratios of the total pixel density of Lhc spots (free and bound to PSII) to those of PsbB and PsbC spots (Figure S4). (C) Changes in the distribution of complexes among their different organizational forms during the treatments. The amounts of complexes are given as the percentage of control values. Means and standard deviation values are provided, and significant differences are indicated by different letters according to ordinary one-way (PSI/PSII), Kruskal-Wallis (LHCII/PSII) (Figure 3B), or Brown-Forsythe and Welch (Figure 3C) ANOVA followed by Tukey’s, Dunn’s, or Dunnett’s T3 multiple comparison post hoc tests ($P \leq 0.05$), respectively ($n = 4$ –15).

3.6 | In vivo analysis of changes in the granum repeat distance values using small-angle neutron scattering

Small-angle neutron scattering (SANS) curves obtained from *C. setosa* plants exhibited scattering features arising from the periodic structure of the grana. After 41 days of drought stress, the diffraction peak was shifted towards higher momentum transfer values, corresponding to a shrinkage of the membrane system (Figure 7A). Comparison of calculated RD values of four dry and three control plants (with at least 3 leaves measured on each plant) confirmed the observation, with an error weighted average of 20.5 nm thylakoid membrane RD observed on control watered plants and 19.5 nm on drought-stressed plants. Detailed calculated RD values are presented in Tables S2 and S3 and indicate some biological variability between the different leaves of the

same plant, as well as between different plants. However, the Welch’s test performed on all data obtained from control (Table S2) and drought-stressed (Table S3) plants indicated significantly lower RD values in the latter (20.5 and 19.3 nm, respectively).

Due to the observed biological variability, we followed the recovery of the thylakoid membranes in the same leaves from the dry stage until 7 days of recovery after re-watering. The drought-induced shrinkage of the thylakoid membranes was (at least partially) reversible; 25 hours and 7 days after re-watering, the slight swelling of the thylakoid membranes was clearly visible (Figure 8). Calculated RD values for two different plants with 2–3 leaves on each plant confirmed this observation (Table 4).

As we can see in Figure 8 and Table 4, a large part of the rewatering-induced swelling already happened within the first day. We followed the kinetics of the rewatering-induced thylakoid

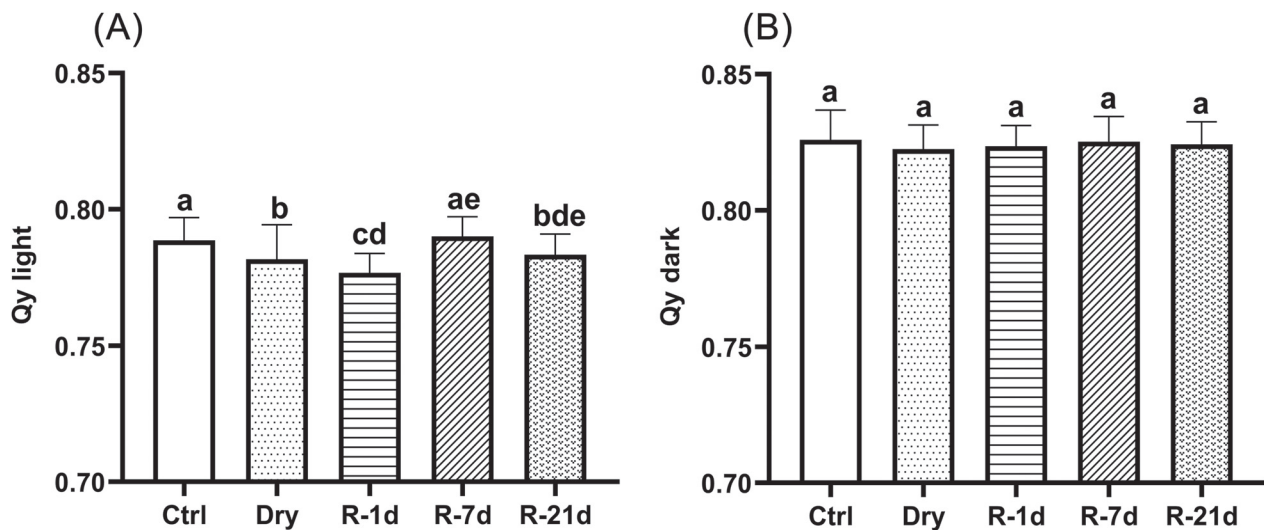


FIGURE 4 Actual (A) and maximal (B) quantum efficiencies of PSII (Q_y light and Q_y dark, respectively) measured in light-adapted or in 20 min dark-adapted *C. setosa* leaves, respectively, after various treatments. Control plants ('Ctrl'), plants exposed to 40–49 days of drought stress ('Dry'); and subsequently recovered *C. setosa* plants ('R-1d', 'R-7d', and 'R-21d') were sampled 1 day, 7 days, and 21 days after re-watering of dry plants, respectively). Mean and standard deviation values are provided; significant differences at $P \leq 0.05$ among treatments are indicated with different letters based on Kruskal-Wallis non-parametric ANOVA followed by Dunn's multiple comparisons post hoc test ($n=20$ –188).

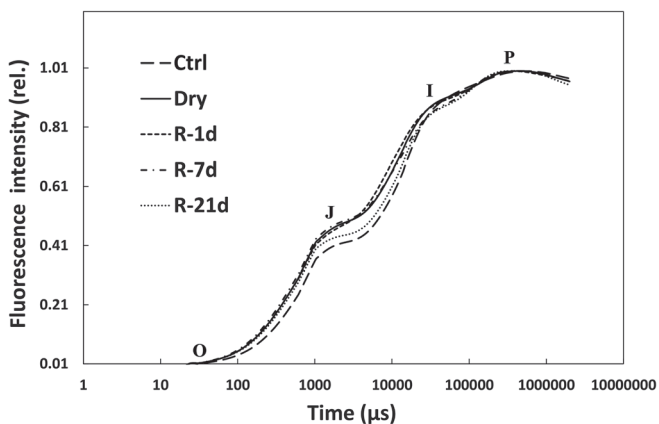


FIGURE 5 Fast chlorophyll *a* fluorescence OJIP transients of the leaves of differently treated *C. setosa* plants. Control plants ('Ctrl'); plants exposed to 40–49 days of drought stress ('Dry'); and subsequently recovered *C. setosa* plants ('R-1d', 'R-7d', and 'R-21d') were sampled 1 day, 7 days, and 21 days after re-watering of dry plants, respectively). Plants were dark-adapted for 20 min before the OJIP transients were recorded, and the transients were double normalized to F_0 and to F_M and then averaged ($n=9$ –20).

membrane swelling in a single leaf of a drought-stressed plant and provided unprecedented time-resolved structural information about this complex membrane system (Figures 9 and S6).

SANS allowed to observe variations of the thylakoid membrane structure across plants and across leaves of individual plants (Tables S2, S3). Our experiments also showed that there is some minor variation in the neutron scattering profile even between different regions of a leaf (Figure 7B), but the RD values were basically identical (18.08 and 18.12 nm) (Table S3).

Variations between leaves of control *C. setosa* plants are also either hardly observable (Figure 7C) or small (Figure 7D) (see also data in Table S2).

Drought-stressed plants may exhibit mainly similar (Figure 7E) or largely differing (Figure 7F) scattering curves across their leaves (see also data in Table S2).

4 | DISCUSSION

According to estimations, approx. 45% of arable lands are subjected to drought worldwide (Abdelraheem et al., 2019), and climate change is only worsening this situation by increasing the duration of the dry periods. Drought stress negatively impacts plant growth, physiology, and reproduction, thus crop yield, resulting in huge economic losses [e.g., €9 billion per year only in the European Union and the United Kingdom (Naumann et al., 2021)]. Photosynthesis is crucial for plant metabolism; thus, it is highly important to understand the effect of drought stress and subsequent re-watering on chloroplast structure and function (Gu et al., 2022). In this wider context, it is relevant to investigate plants that can survive long drought periods and recover after them. Studying such resilient plants can provide insights into improving crop resistance to drought stress.

C. setosa is a tropical ornamental plant known for its ability to maintain photosynthetic activity almost unchanged during drought periods as long as 60 days (Saglam et al., 2008; Nar et al., 2009). Similarly to those analyses (Nar et al., 2009) we also revealed no significant changes in the photosynthetic pigment composition (Table 2) and the electron transport processes.

The maximum quantum efficiency of PSII as measured by Q_y dark was unchanged, while slight changes were observed in the structural dynamics as well as the photochemical activity of PSII in the light-

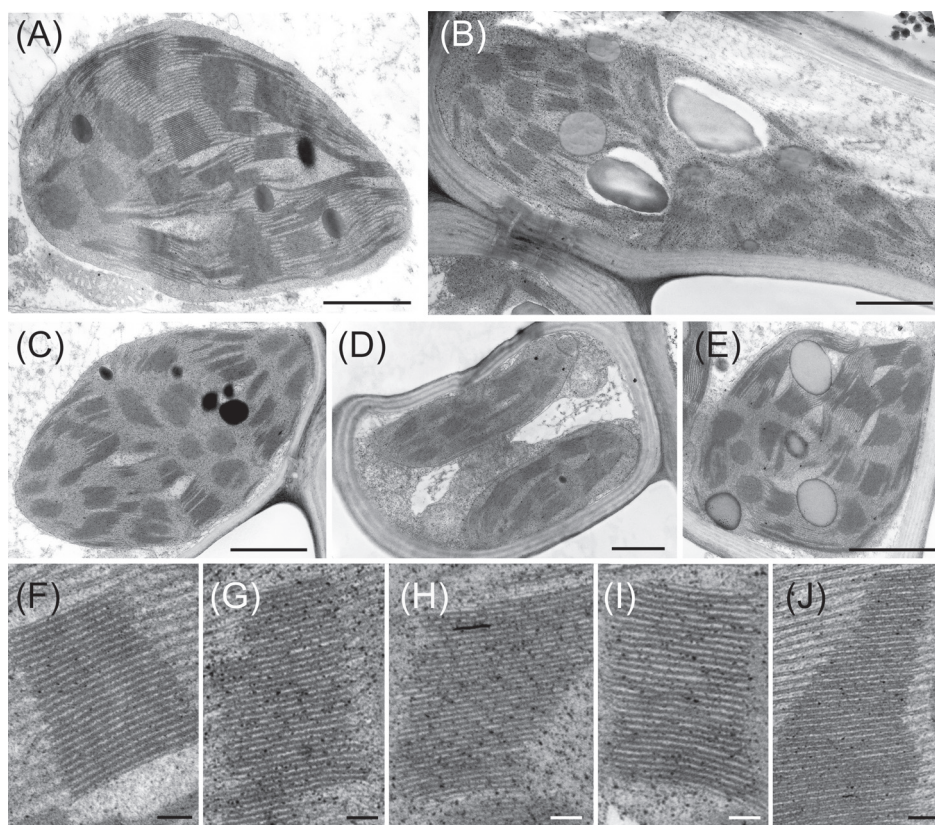


FIGURE 6 Chloroplast (A-E) and granum (F-J) ultrastructure in the mesophyll cells of the middle intervenial regions of leaves of differently treated *C. setosa* plants. (A and F) control 1 plant ('Ctrl 1 leaf 1'); (B and G) control 2 plant ('Ctrl 2 leaf 1'); (C and H) 49-day drought-stressed leaf, region one ('Dry-49, leaf 1, region 1'); (D, E and I, J) leaves of the 49-day drought-stressed plant after 18 h recovery (D and I) and 21-day recovery (E and J), respectively. Scale bar: 1 μm (A-E) and 100 nm (F-J).

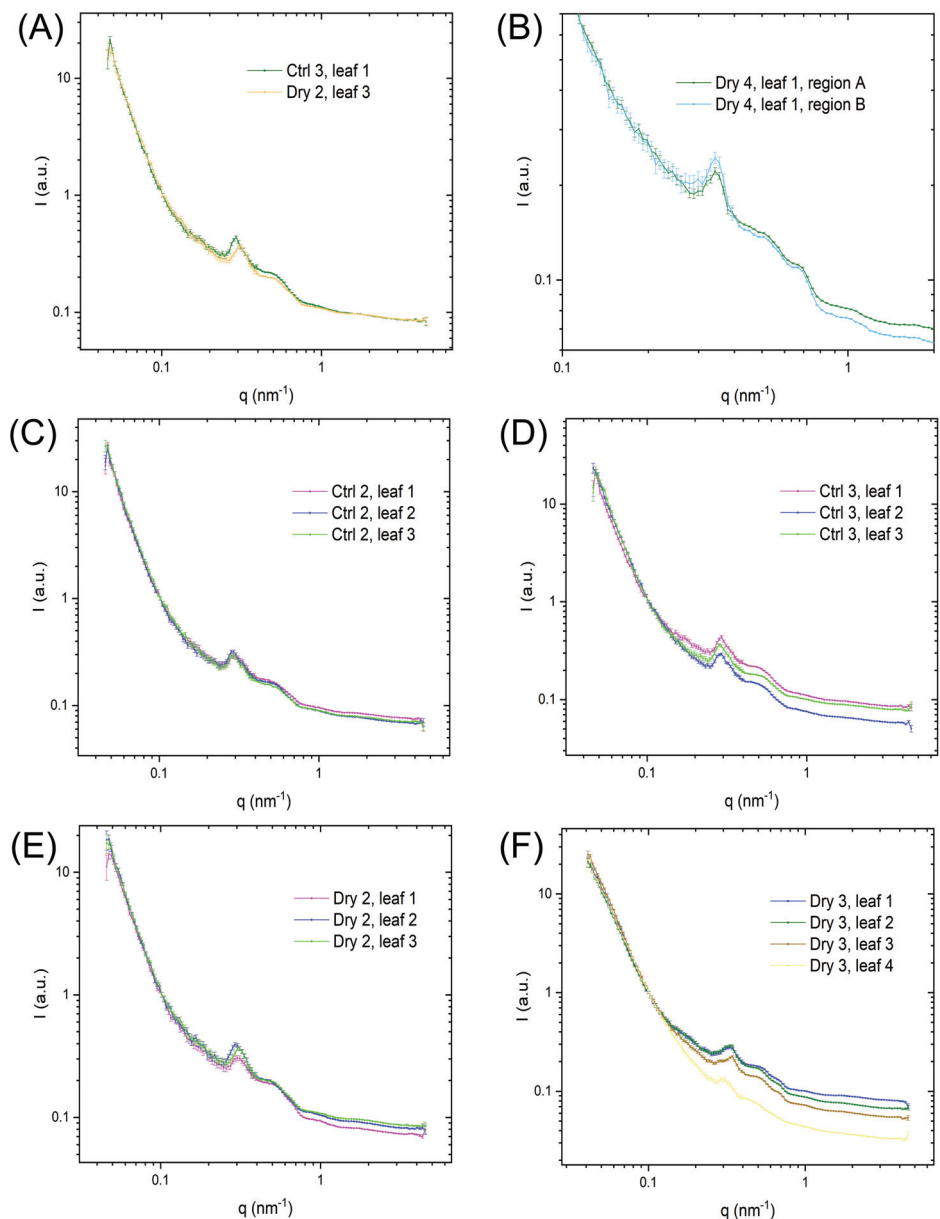
TABLE 3 Granum repeat distance (RD) values of the leaf chloroplasts of control and drought-stressed *C. setosa* plants as obtained by TEM analyses. 'Ctrl 1-3': data obtained from analyzing control leaves from three different plants (data from 'Ctrl 1, leaf 1' and 'Ctrl 2, leaf 1' originate from the samples also shown in Figure 6A,B, respectively); 'Dry-45 1, leaf 1' and 'Dry-45 1, leaf 2': two different leaves from a 45-day drought-stressed plant; 'Dry-49 leaf 1, region 1' and 'Dry-49 leaf 1, region 2': two different leaf regions sampled from the same leaf of a 49-day drought-stressed plant; 'R-18h, leaf 2' and 'R-21d, leaf 3': two different leaves of the 49-day drought-stressed plant ('Dry-49') sampled after 18 h and 21 days of recovery, respectively. RD values were determined by Fast Fourier Transformation performed in ImageJ on electron microscopic images. Mean and standard error values are provided. Different letters indicate statistically significant differences across the samples based on Kruskal-Wallis non-parametric ANOVA followed by Dunn's multiple comparisons post hoc test ($P \leq 0.05$) ($n = 88$ -182).

	Repeat distance (nm)
Ctrl 1, leaf 1 (n=118)	16.36 \pm 0.14 ^{ab}
Ctrl 2, leaf 1 (n=115)	17.87 \pm 0.18 ^c
Ctrl 3, leaf 1 (n=94)	18.97 \pm 0.17 ^d
Dry-45 1, leaf 1 (n=182)	16.00 \pm 0.08 ^a
Dry-45 1, leaf 2 (n=96)	16.44 \pm 0.14 ^{ab}
Dry-49, leaf 1, region 1 (n=122)	16.40 \pm 0.13 ^{ab}
Dry-49, leaf 1, region 2 (n=88)	17.36 \pm 0.10 ^{ce}
R-18h, leaf 2 (n=159)	16.99 \pm 0.15 ^{be}
R-21d, leaf 3 (n=108)	16.99 \pm 0.21 ^{be}

adapted state under drought stress (Figure 4). This indicates that the dark-adapted photosynthetic apparatus has similar functional parameters even under drought stress; however, upon constant illumination, the photochemical processes are somewhat hindered due to other potential fates of the absorbed energy (e.g., non-photochemical quenching occurring due to acceptor-side limitations such as for example stomatal closure resulting in the inhibition of CO₂ fixation). Although OJIP curves may be slightly influenced by the optical properties of the leaves, we observed significantly increased Chl fluorescence (F_M) in the drought-stressed leaves (Table S1), and also a relative increase in the J and I points of the OJIP curve (Figure 5 and Table S1), indicating potential alterations in the plastoquinone pool and the electron flow to PSI; but these changes were reversible after rehydration. Similar drought-induced alterations were reported in the OJIP curves of orchid epiphytes (Zampirolo et al., 2021).

To characterize the thylakoid features, we analyzed for the first time the 77K fluorescence emission spectra of the *C. setosa* leaves and demonstrated no significant changes in the fluorescence of the chlorophyll-protein complexes during drought stress and subsequent recovery (Figure 2). The maximum of the spectra was at a relatively long wavelength (748 nm), which arises from the red forms in light-harvesting complex I (LHCI) associated with photosystem I (LHCI-PSI), which were shown to be species-specific (Bos et al., 2023). Similar long-wavelength fluorescence emission (at around 742 nm) was typical for young leaves of common ash and horse chestnut (Solymosi et al., 2012).

FIGURE 7 Biological variability of SANS signals obtained from *C. setosa* leaves. (A) Typical small-angle neutron scattering (SANS) signal (intensity – I) of one of the leaves of control ('Ctrl') and of a 41-day drought-stressed ('Dry') *C. setosa* plant. The numbers after 'Ctrl' and 'Dry' and after 'leaf' refer to given plants and their specific leaves, respectively. (B) Intraleaf structural variations of the grana in leaf 1 of a 41-day drought-stressed plant ('Dry 4') observed with SANS. Region A and B correspond to different regions of leaf 1. (C–D) Variations between the SANS scattering curves of the leaves (numbered with different numbers) of control ('Ctrl') plants from two different plants: (C) 'Ctrl 3' plant, and (D) 'Ctrl 2' plant. (E–F) Variations between the SANS scattering curves of leaves of 41-day drought-stressed ('Dry') plants from two different plants: (E) 'Dry 2' plant, and (F) 'Dry 3' plant.



To follow the variations in thylakoid complex organization during drought stress and recovery, we also performed, for the first time, an in-depth analysis of the chlorophyll-protein complexes of *C. setosa* by BN gel electrophoresis during drought stress and recovery. In different plant species, PSII is usually the most sensitive to drought stress. In *Arabidopsis*, together with a decrease in Chl content, a significant reduction in the amounts of PSII supercomplexes (PSII-s) and more free LHCII were observed at 20% RWC by BN or Clear Native (CN) PAGE (Chen et al., 2016; Hu et al., 2023). Similar organizational changes of thylakoids were detected in drought-stressed pea plants around 30% RWC, where the level of PSII-s was significantly lowered and those of LHCII and PSII monomers (PSII-m) rose, which was accompanied by increased RD values of the grana as measured by TEM (Pandey et al., 2023). Though the Chl content was only reduced slightly, dissociation of LHCII from PSII-s was also found in the homoiochlorophyllous resurrection species *Haberlea*

rhodopensis, in similar extent both at 50 and 8% RWC (Sárvári et al., 2014).

The behaviour of *C. setosa*, however, differed from the more general drought-induced changes in thylakoid organization. The increased amount of PSII-s together with the lowering of PSII-m (and that of some LHCII-t) without any change in the leaf Chl content during the long drying period reaching about 60% RWC (Figure 3 and Table 2) may refer to differences in the organization of the PSII pool. These changes were parallel to a decrease in the RD values of granum thylakoids (Tables 3, S2 and S3). Interestingly, different PSII organization was also found depending on the water loss in the freeze-fractured leaf tissues of the resurrection plant *Craterostigma pumilum* by cryo-scanning electron microscopy: PSII complexes were present at lower than control density and in semicrystalline arrays in the thylakoids at 15–25% and 5–10% RWC, respectively (Charuvi et al., 2015). Accompanying the increase in the proportion

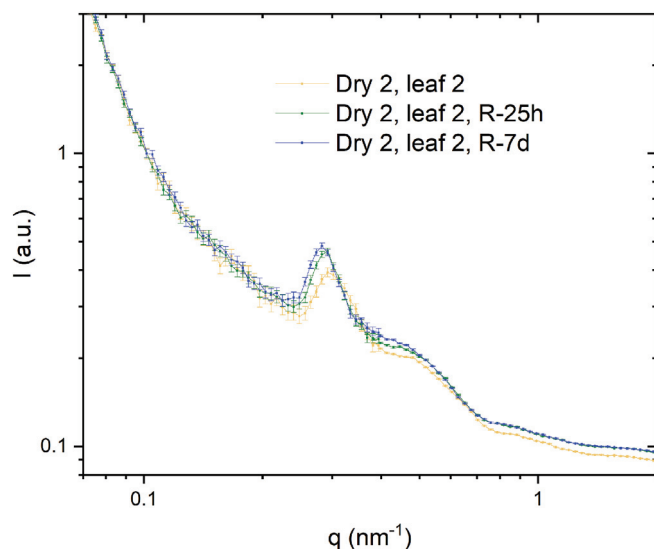


FIGURE 8 Effect of re-watering on the SANS signal of a leaf of a 41-day drought-stressed *C. setosa* plant (labelled as ‘Dry 2’). ‘Dry 2, leaf 2’: leaf labelled as 2 measured after drought stress; ‘R-25h’ and ‘R-7d’: same leaf of the same, drought-stressed plant sampled after 25 h and 7 days of recovery, respectively.

TABLE 4 Effect of re-watering on the repeat distance values of the grana in various leaves of 41-day drought-stressed (‘Dry’) *C. setosa* plants. The numbers after ‘Dry’ and after ‘leaf’ refer to given plants and their specific leaves, respectively. ‘Dry’: leaves from 41-day drought-stressed plants; ‘R-25h’ and ‘R-7d’: leaves of the above drought-stressed plant sampled after 25 h and 7 days of recovery, respectively. SANS curves represent statistically averaged information over the entire sample volume in the neutron beam. RD values are calculated from the fitting results of the SANS curves. Error bars are derived via error propagation from the error of the mean of the fitted skewed normal distribution.

	Repeat distance (nm)		
	Dry	R-25h	R-7d
Dry 1, leaf 1	19.82 ± 0.02	20.76 ± 0.03	20.95 ± 0.01
Dry 1, leaf 2	20.08 ± 0.04	20.69 ± 0.02	20.75 ± 0.01
Dry 1, leaf 3	20.17 ± 0.03	20.53 ± 0.02	20.72 ± 0.01
Dry 2, leaf 2	20.33 ± 0.02	20.94 ± 0.01	21.28 ± 0.01
Dry 2, leaf 3	19.49 ± 0.02	20.56 ± 0.01	21.12 ± 0.01

of PSII-s, a significant decrease in the amounts of PSI-LHCII complexes was observed in thylakoids of the dried *C. setosa*, similarly to drought-stressed *H. rhodopensis* (Sárvári et al., 2014). Though this complex is very sensitive to solubilization (Sárvári et al., 2022), the clear trend of its change during the drought and recovery treatments refers to a varied PSI organization, too.

In parallel with physiological and organizational changes, we also reported (ultra)structural alterations of *C. setosa* plants during drought stress and recovery. To the best of our knowledge, this is the first time the thylakoid organization of a higher plant during drought stress is

analysed by SANS under fully *in vivo* conditions. Earlier data studying the RD of the thylakoid lamellae in a desiccated desert crust cyanobacterium pointed to the loss of thylakoid regularity upon drought stress (Bar Eyal et al., 2017). However, it should be noted that cyanobacteria and higher plants have completely differently organized thylakoid systems. On the other side, in contrast to our data, the photosynthetic activity was very quickly recovered in the cyanobacterium after rehydration (Bar Eyal et al., 2017).

The thickness of the water-storing adaxial hypodermis cell layer significantly decreased during drought stress resulting in the decrease of the entire leaf width, in accordance with observations of Kutlu et al. (2009), but was restored already 18 h after re-watering (Figure 1 and Table 1). This indicates leaf succulence in the species. Chloroplast length decreased significantly under drought stress, but was also already restored after 18 h (Table 1). No important and specific changes were observed in chloroplast ultrastructure during the treatments (Figure 6). Surprisingly, significant differences were observed between the RD values of the studied leaves of three control plants (Table 3), probably due to the large biological variability observed also by SANS (Figure 7). We have also found significant differences even within the RD values of the same leaf’s different neighbouring interveinal middle leaf regions (Table 3). This indicates that at the nano-scale level, quantitative TEM analyses might have their own limitations. Therefore, and also due to its invasive sampling, the TEM method was not really suitable for reliably determining the changes of the RD values of individual leaves during drought stress and subsequent recovery. When we compared all analyzed control and drought-stressed leaves, the significant decrease in RD values was confirmed; however, this required the completion of time-consuming and expensive TEM analyses on several biological replicates. Even this way, TEM only provided information on very small areas of a given leaf in contrast to SANS, which collects averaged information about grana from much larger leaf areas. On the other side, TEM has its own advantages as it provides information on cellular integrity and ultrastructure way beyond granum RD values.

Previous data on the effects of drought stress on chloroplast ultrastructure in other species are somewhat conflicting: in most cases, swelling of the lumen is reported as a consequence of drought stress (e.g., Shao et al., 2016; Pandey et al., 2023), while in other cases swelling was not observed in drought-sensitive crops (e.g., Ounoki et al., 2021) as well as in desiccation-tolerant plants (Georgieva et al., 2017; Mihailova et al., 2022). The often reported swelling may be an artefact arising from osmotic changes during chemical fixation or changes in membrane permeability, and RD values measured on electron micrographs provide information only on a limited number of grana in an invasive way. Based on our analyses, TEM does not seem to be suitable to monitor small changes in RD values in samples with high biological variability. Therefore, we introduced a novel, fully *in vivo* method to obtain statistically averaged information about the RD of the granum thylakoid membranes under drought stress. Due to the non-invasive nature of the SANS technique, this information corresponds to the intact live state of the plant leaves, which is of especially high value when the influence of the abundance or the lack of

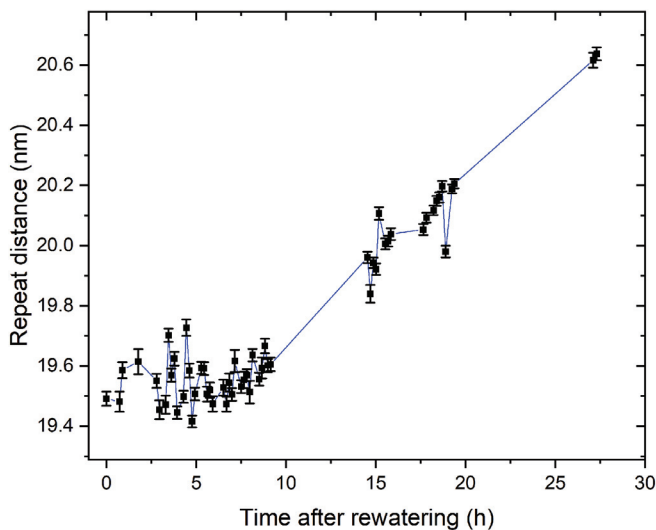


FIGURE 9 Kinetics of the rewatering-induced swelling of the grana in the leaf of a 41-day drought-stressed *C. setosa* plant ('Dry 2, leaf 3'). The error bars are derived from the error of the mean of the skewed normal distribution in the fitting results (see equation in Methods S2).

water is studied in plant systems (Gu et al., 2022). All the structural characterization tools widely used to observe nanoscale features in plant systems are prone to alter the water content of the sample (including cryo-techniques using cryo-preserving agents). The unique nature of the SANS technique allows not only unaltered observation of thylakoid membrane structures in drought-stressed plant leaves but is also capable of following thylakoid membrane reorganizations in individual leaves upon re-watering of the living plants. Also, it may provide a fast, non-invasive and better insight into the native biological variability among plants, their individual leaves, and different regions of the same leaf (Figure 7B). Unfortunately, most plants measured so far have no clear SANS scattering profile without infiltration of their leaves with D_2O (Ünnep et al., 2014a, 2014b; Karlsson et al., 2015; Ünnep et al., 2020; Nagy & Garab, 2021). In this respect, in addition to its extreme drought tolerance, *C. setosa* was also uniquely suitable for *in vivo* SANS measurements as it had clearly detectable SANS membrane diffraction peaks without any invasive pretreatment. Its suitability to SANS measurements might be related to the fact that it has relatively large and regular grana built by several (sometimes up to 20-40) thylakoid layers. In addition, it is a relatively small plant that can be positioned within the SANS sample environment such that only the leaves are exposed to the neutron beam while the pot remains outside.

Thanks to the exceptional wavelength resolution of the EQ-SANS instrument, we were able to observe some hereto not observed features in the SANS curves of the intact leaves, especially the asymmetric nature of the first-order Bragg peak corresponding to the periodic thylakoid membranes. During the fitting of the data, we captured this with a skewed normal distribution component. This asymmetric peak may be reasoned by considering the apparent upper limit for the repeat distance (RD) of the thylakoid membranes in the case of well-

hydrated membranes (see Figure 7A), beyond which the periodic membrane system would be too loose to maintain structural integrity. Similarly, the skewed normal distribution in the case of drought-stressed membranes suggests the existence of a lower limit for the RD determined by physical constraints for the compression of adjacent membranes due to the protein subunits protruding into the interthylakoidal and luminal aqueous phases (see e.g., Figure 7F).

In spite of the observed individual variabilities of RD values among leaves and leaf regions (Tables 4, S2 and S3 and Figure 7C-F), we have clearly observed with SANS a significant shrinkage of the granum thylakoids upon drought stress, and the fast recovery of the RD values in the same leaf 25 h after re-watering (Figures 7A and 8-9, Table 4). The granum RD values comprise the width of two thylakoid membranes, the thylakoid lumen and the interthylakoidal region (also called partition gap) (Mazur et al., 2021; Gu et al., 2022). Thus, the observed ca. 1 nm decrease in RD values from approx. 20.5 nm to 19.5 nm (Table 4, S2 and S3) must be associated with water loss either by the thin partition gap filled with stromal fluids or, more probably, by the thylakoid lumen during dehydration. Water uptake upon rehydration might only be a first step towards higher structural flexibility of the grana and the potential restoration of the photosynthetic apparatus occurring on a longer time scale. Li et al. (2020) observed slight swelling of the lumen of dark-adapted plants upon illumination, while a minor but still significant decrease was reported for the thickness of the partition gap and also the thylakoid membrane. Changes in the lumen's thickness could influence the mobility and activity of various proteins present in the lumen (e.g., plastocyanin, violaxanthin de-epoxidase, DEG proteases or even the oxygen evolving complex), while changes in the partition gap may affect the 'PSII sandwiches', i.e. the PSII-LHCII complexes present in an opposite way in adjacent thylakoids (Kirchhoff et al., 2011; Li et al., 2020). Due to the function of these various proteins, the above changes may affect photosynthetic activity as well as photoprotective and repair mechanisms of the grana.

The series of scattering curves presented in Figure 7F deserves special attention. According to our interpretation, this plant – possibly due to reaching the limitation of its water reserves – distributed water to different extents into its leaves. Though the scattering curves are not presented in absolute scale, decreasing values of the incoherent background at the high momentum transfer end of the scattering curves suggest decreasing water content from 'Dry 3, leaf 1' towards leaf 4 of the same plant ('Dry 3, leaf 4'). The clear separation of diffraction peaks is also apparent at ca. 0.5 and 0.7 nm^{-1} . These two peaks do not clearly separate in control or even in less drought-stressed plants, most probably due to the polydispersity of the transmembrane structural parameters in the presence of excess water. The crystallin-like sharp scattering features are also notable, e.g., on 'Dry 3, leaf 3' (Figure 7F), which can be understood when the limited water volume induced upper limits and the protein composition imposed lower limits of the thylakoid membrane RD are expected to be converging. A possible additional level of water depletion can be seen at 'Dry 3, leaf 4', where the lack of sufficient volume of aqueous phases between adjacent thylakoid membranes (in the luminal and/or interthylakoidal space) is proposed

to result in the lack of sufficient contrast and hence the diminishment of well discernable scattering features.

Taken together, due to – among others – the water storage capacity of its hypodermal cells, *C. setosa* is relatively well maintaining the chlorophyll content, native organization, structure and functioning of its chloroplasts even at severe drought stress (40–49 days of water withdrawal, 60% leaf RWC) and recovers functional activity after 7 or 21 days of re-watering. We have also clearly demonstrated that, in contrast to TEM, the SANS method is uniquely capable of providing dynamic insight into *in vivo* changes in the organization of the granum thylakoid membranes of the same leaf at the nanoscale level, overcoming the otherwise observed intraleaf regional variabilities, as well as biological variability among different leaves of the same plant. It also has the advantage of monitoring the shrinkage and fast restoration of the granum membranes on a relatively short time scale.

AUTHOR CONTRIBUTIONS

KS conceived and designed the experiments. ÉS performed gel electrophoresis and pigment content measurements, RÜ and GN performed and analyzed SANS, KS performed light microscopy and TEM, all other measurements and related data analyses and all statistical analyses were performed by RH. KS and RH wrote the manuscript with input from all authors.

ACKNOWLEDGEMENTS

The authors are grateful to Győző Garab and Zsuzsanna Várkonyi (HUN-REN Biological Research Center, Szeged, Hungary) and to Nihal Kutlu and Asim Kadioglu (Karadeniz Technical University, Trabzon, Türkiye) for the idea to use *C. setosa* plant in our experiments. The authors would like to thank Tünde Szabó-Szöllősi and László Papp (Botanical Garden of ELTE, Budapest, Hungary) for providing the plant material for the experiments. We are grateful to Csilla Gergely (ELTE) for TEM and LM embedding and sectioning and Györgyi Balogh (ELTE) for her technical assistance with gel electrophoresis. We would like to thank Gusztáv Schay (Sемmelweis University, Budapest, Hungary) for advice on statistical analyses. A portion of this research used resources at the Spallation Neutron Source, a DOE Office of Science User Facility operated by the Oak Ridge National Laboratory. The beam time was allocated to EQ-SANS on proposal numbers IPTS-26180.1 and 27426.1. G.N. is grateful to Mary-Ellen Donnelly (ORNL and Canadian Light Source Inc., Canada) for her help in the acclimation of the plants. We would like to thank the Paul Scherrer Institute (PSI), Villigen, Switzerland, for providing us beamtime for the SANS experiments on the SANS-II beam-line at the Swiss Spallation Neutron Source SINQ for preliminary measurements checking the signal of intact *C. setosa* plants. This work was financed by the OTKA FK 124748 research grant of the National Research, Development, and Innovation Office (NRDIO). The work of U.R. was also financed from the OTKA PD 138540 grant. K.S. would like to thank the support from the Bolyai János Research Scholarship of the Hungarian Academy of Sciences and from the ÚNKP-23-5 New National Excellence Program from the source of the National Research, Development, and Innovation Fund. R.H. is grateful

to Tempus Public Foundation (Hungary) for the Stipendium Hungaricum Ph.D. Scholarship.

FUNDING INFORMATION

Nemzeti Kutatási Fejlesztési és Innovációs Hivatal, Grant/Award Numbers: FK124748, PD138540; Nemzeti Kutatási, Fejlesztési és Innovációs Alap, Grant/Award Number: New National Excellence Program ÚNKP-23-5-ELTE-12; Tempus Közalapítvány, Grant/Award Number: Stipendium Hungaricum Scholarship to R.H.

DATA AVAILABILITY

The data that support the findings of this study are available upon reasonable request from the corresponding author.

ORCID

Richard Hembrom  <https://orcid.org/0000-0002-1758-8950>

Renáta Ünneper  <https://orcid.org/0000-0001-5916-1974>

Éva Sárvári  <https://orcid.org/0000-0003-1416-1860>

Gergely Nagy  <https://orcid.org/0000-0003-2742-0198>

Katalin Solymosi  <https://orcid.org/0000-0001-5246-2547>

REFERENCES

- Abdelraheem, A., Esmaili, N., O'Connell, M., & Zhang, J. (2019). Progress and perspective on drought and salt stress tolerance in cotton. *Industrial Crops and Products*, 130, 118–129.
- Adolfsson, L., Solymosi, K., Andersson, M. X., Keresztes, Á., Uddling, J., Schoefs, B., & Spetea, C. (2015). Mycorrhiza symbiosis increases the surface for sunlight capture in *Medicago truncatula* for better photosynthetic production. *PLOS ONE*, 10(1), e0115314.
- Almásy, L. (2021). New measurement control software on the Yellow Submarine SANS instrument at the Budapest Neutron Centre. *Journal of Surface Investigation: X-Ray, Synchrotron and Neutron Techniques*, 15(3), 527–531.
- Arnold, O., Bilheux, J. C., Borreguero, J. M., Buts, A., Campbell, S. I., Chapon, L., Doucet, M., Draper, N., et al. (2014). Mantid—Data analysis and visualization package for neutron scattering and μ SR experiments. *Nuclear Instruments and Methods in Physics Research Section A: Accelerators, Spectrometers, Detectors and Associated Equipment*, 764, 156–166.
- Ayaz, F. A., Kadioglu, A., & Dogru, A. (2001). Leaf rolling effects on lipid and fatty acid composition in *Ctenanthe setosa* (Marantaceae) subjected to water-deficit stress. *Acta Physiologiae Plantarum*, 23(1), 43–47.
- Bai, J. P., Gao, H. J., Yang, H. Y., Lou, Y., Zhang, J. L., Wang, D., & Zhang, J. L. (2016). Comparison of ultrastructural and physiological changes of potato (*Solanum tuberosum* L.) plantlets subjected to salt and modeling drought stresses. *Acta Physiologiae Plantarum*, 38(7), 182.
- Bar Eyal, L., Ranjbar Choubeh, R., Cohen, E., Eisenberg, I., Tamburu, C., Dorogi, M., Ünneper, R., Appavou, M.-S., et al. (2017). Changes in aggregation states of light-harvesting complexes as a mechanism for modulating energy transfer in desert crust cyanobacteria. *Proceedings of the National Academy of Sciences*, 114(35), 9481–9486.
- Basu, S., Ramegowda, V., Kumar, A., & Pereira, A. (2016). Plant adaptation to drought stress. *F1000Research*, 5, 1554.
- Bhargava, S., & Sawant, K. (2013). Drought stress adaptation: Metabolic adjustment and regulation of gene expression. *Plant Breeding*, 132(1), 21–32.
- Bos, P. R., Schiphorst, C., Kercher, I., Buis, S., de Jong, D., Vunderink, I., & Wientjes, E. (2023). Spectral diversity of photosystem I from flowering plants. *Photosynthesis Research*, 155(1), 35–47.

- Charuvi, D., Nevo, R., Shimoni, E., Naveh, L., Zia, A., Adam, Z., Farrant, J. M., Kirchoff, H., & Reich, Z. (2015). Photoprotection conferred by changes in photosynthetic protein levels and organization during dehydration of a homoiochlorophyllous resurrection plant. *Plant Physiology*, 167(4), 1554–1565.
- Chen, D., Wang, S., Qi, L., Yin, L., & Deng, X. (2018). Galactolipid remodeling is involved in drought-induced leaf senescence in maize. *Environmental and Experimental Botany*, 150, 57–68. <https://doi.org/10.1016/j.envexpbot.2018.02.017>
- Chen, Y. E., Liu, W. J., Su, Y. Q., Cui, J. M., Zhang, Z. W., Yuan, M., Zhang, H. Y., & Yuan, S. (2016). Different response of photosystem II to short and long-term drought stress in *Arabidopsis thaliana*. *Physiologia Plantarum*, 158(2), 225–235.
- Farooq, M., Wahid, A., Kobayashi, N., Fujita, D., & Basra, S. M. A. (2009). Plant drought stress: Effects, mechanisms and management. In E. Lichtfouse, M. Navarrete, P. Debaeke, S. Véronique, & C. Alberola (Eds.), *Sustainable Agriculture* (pp. 153–188). Springer, Netherlands.
- Füzi, J., Len, A., & Bajnok, K. (2017). *Research instruments at the Budapest Neutron Centre: Handbook of the Central European Training School on neutron techniques*. KFKI, Hungary.
- Garab, G., Magyar, M., Sipka, G., & Lambrev, P. H. (2023). New foundations for the physical mechanism of variable chlorophyll a fluorescence. Quantum efficiency versus the light-adapted state of photosystem II. *Journal of Experimental Botany*, 74(18), 5458–5471.
- Georgieva, K., Solti, Á., Mészáros, I., Keresztes, Á., & Sárvári, É. (2017). Light sensitivity of *Haberlea rhodopensis* shade adapted phenotype under drought stress. *Acta Physiologiae Plantarum*, 39(8), 164.
- Giardi, M. T., Cona, A., Geiken, B., Kučera, T., Masojádek, J., & Mattoo, A. K. (1996). Long-term drought stress induces structural and functional reorganization of photosystem II. *Planta*, 199(1), 118–125.
- Griffiths, H., & Males, J. (2017). Succulent plants. *Current Biology*, 27(17), R890–R896.
- Gu, L., Grodzinski, B., Han, J., Marie, T., Zhang, Y.-J., Song, Y. C., & Sun, Y. (2022). Granal thylakoid structure and function: Explaining an enduring mystery of higher plants. *New Phytologist*, 236(2), 319–329.
- Heller, W. T., Cuneo, M., Debeer-Schmitt, L., Do, C., He, L., Heroux, L., Littrell, K., Pingali, S. V., et al. (2018). The suite of small-angle neutron scattering instruments at Oak Ridge National Laboratory. *Journal of Applied Crystallography*, 51(2), 242–248.
- Heller, W. T., Hetrick, J., Bilheux, J., Calvo, J. M. B., Chen, W.-R., DeBeer-Schmitt, L., Do, C., Doucet, M., et al. (2022). drtsans: The data reduction toolkit for small-angle neutron scattering at Oak Ridge National Laboratory. *SoftwareX*, 19.
- Hu, C., Elias, E., Nawrocki, W. J., & Croce, R. (2023). Drought affects both photosystems in *Arabidopsis thaliana*. *New Phytologist*, 240(2), 663–675.
- Johnson, M. P., & Wientjes, E. (2020). The relevance of dynamic thylakoid organisation to photosynthetic regulation. *Biochimica et Biophysica Acta (BBA) - Bioenergetics*, 1861(4), 148039.
- Kalaji, H. M., Schansker, G., Brestic, M., Bussotti, F., Calatayud, A., Ferroni, L., Goltsev, V., Guidi, L., et al. (2017). Frequently asked questions about chlorophyll fluorescence, the sequel. *Photosynthesis Research*, 132(1), 13–66.
- Karlsson, P. M., Herdean, A., Adolfsson, L., Beebo, A., Nziengui, H., Irigoyen, S., Ünneper, R., Zsiros, O., et al. (2015). The *Arabidopsis* thylakoid transporter PHT4;1 influences phosphate availability for ATP synthesis and plant growth. *The Plant Journal*, 84(1), 99–110.
- Kebbas, S., Lutts, S., & Aid, F. (2015). Effect of drought stress on the photosynthesis of *Acacia tortilis* subsp. *Raddiana* at the young seedling stage. *Photosynthetica*, 53(2), 288–298.
- Kirchoff, H. (2019). Chloroplast ultrastructure in plants. *New Phytologist*, 223(2), 565–574.
- Kirchoff, H., Hall, C., Wood, M., Herbstová, M., Tsabari, O., Nevo, R., Charuvi, D., Shimoni, E., & Reich, Z. (2011). Dynamic control of protein diffusion within the granal thylakoid lumen. *Proceedings of the National Academy of Sciences*, 108(50), 20248–20253.
- Kluyver, T., Ragan-Kelley, B., Pérez, F., Granger, B., Bussonnier, M., Frederic, J., Kelley, K., Hamrick, J., et al. & Jupyter development team. (2016). *Jupyter Notebooks – a publishing format for reproducible computational workflows*. In F. Loizides & B. Schmidt (Eds.), (pp. 87–90). IOS Press.
- Kutlu, N., Terzi, R., Tekeli, Ç., Şenel, G., Battal, P., & Kadioğlu, A. (2009). Changes in anatomical structure and levels of endogenous phytohormones during leaf rolling in *Ctenanthe setosa* under drought stress. *Turkish Journal of Biology*, 33(2), 115–122.
- Li, M., Mukhopadhyay, R., Svoboda, V., Oung, H. M. O., Mullendore, D. L., & Kirchoff, H. (2020). Measuring the dynamic response of the thylakoid architecture in plant leaves by electron microscopy. *Plant Direct*, 4(11), e00280.
- Lichtenthaler, H. K. (1987). Chlorophylls and carotenoids: Pigments of photosynthetic biomembranes. *Methods in Enzymology* (148), 350–382.
- Mazur, R., Mostowska, A., & Kowalewska, Ł. (2021). How to measure grana – ultrastructural features of thylakoid membranes of plant chloroplasts. *Frontiers in Plant Science*, 12, 756009.
- Mihailova, G., Christov, N. K., Sárvári, É., Solti, Á., Hembrom, R., Solymosi, K., Keresztes, Á., Velitchkova, M., Popova, A. V., Simova-Stoilova, L., Todorovska, E., & Georgieva, K. (2022). Reactivation of the photosynthetic apparatus of resurrection plant *Haberlea rhodopensis* during the early phase of recovery from drought- and freezing-induced desiccation. *Plants*, 11(17), 2185.
- Murata, N., Nishimura, M., & Takamiya, A. (1966). Fluorescence of chlorophyll in photosynthetic systems III. Emission and action spectra of fluorescence—Three emission bands of chlorophyll a and the energy transfer between two pigment systems. *Biochimica et Biophysica Acta (BBA) - Biophysics Including Photosynthesis*, 126(2), 234–243.
- Nagy, G., & Garab, G. (2021). Neutron scattering in photosynthesis research: Recent advances and perspectives for testing crop plants. *Photosynthesis Research*, 150(1), 41–49.
- Nar, H., Saglam, A., Terzi, R., Várkonyi, Z., & Kadioğlu, A. (2009). Leaf rolling and photosystem II efficiency in *Ctenanthe setosa* exposed to drought stress. *Photosynthetica*, 47(3), 429–436.
- Naumann, G., Cammalleri, C., Mentaschi, L., & Feyen, L. (2021). Increased economic drought impacts in Europe with anthropogenic warming. *Nature Climate Change*, 11(6), 485–491.
- Nuccio, M. L., Rhodest, D., McNeil, S. D., & Hanson, A. D. (1999). Metabolic engineering of plants for osmotic stress resistance. *Current Opinion in Plant Biology*, 2(2), 128–134.
- Osakabe, Y., Osakabe, K., Shinozaki, K., & Tran, L. S. P. (2014). Response of plants to water stress. *Frontiers in Plant Science*, 5, 00086.
- Ounoki, R., Agh, F., Hembrom, R., Ünneper, R., Szögi-Tatár, B., Böszörményi, A., & Solymosi, K. (2021). Salt stress affects plastid ultrastructure and photosynthetic activity but not the essential oil composition in Spearmint (*Mentha spicata* L. var. *Crispa* “Moroccan”). *Frontiers in Plant Science*, 12(739467), 1–18.
- Pandey, J., Devadasu, E., Saini, D., Dhokne, K., Marriboina, S., Raghavendra, A. S., & Subramanyam, R. (2023). Reversible changes in structure and function of photosynthetic apparatus of pea (*Pisum sativum*) leaves under drought stress. *The Plant Journal*, 113(1), 60–74.
- Porra, R. J., Thompson, W. A., & Kriedemann, P. E. (1989). Determination of accurate extinction coefficients and simultaneous equations for assaying chlorophylls a and b extracted with four different solvents: Verification of the concentration of chlorophyll standards by atomic absorption spectroscopy. *Biochimica et Biophysica Acta (BBA) - Bioenergetics*, 975(3), 384–394.
- Rantala, M., Rantala, S., & Aro, E. M. (2020). Composition, phosphorylation and dynamic organization of photosynthetic protein complexes in plant thylakoid membrane. *Photochemical & Photobiological Sciences*, 19(5), 604–619.
- Saglam, A., Kadioğlu, A., Terzi, R., & Saruhan, N. (2008). Physiological changes in them in post-stress emerging *Ctenanthe setosa* plants under drought conditions. *Russian Journal of Plant Physiology*, 55(1), 48–53.

- Saglam, A., Kalaycioglu, E., Guven, F. G., Saruhan, N., Kadioglu, A., & Demiralay, M. (2014). Hydrogen peroxide extends postharvest life of *Ctenanthe setosa* leaf cuts under osmotic stress by reducing leaf rolling. *Horticulture, Environment, and Biotechnology*, 55(4), 308–314.
- Sapeta, H., Costa, J. M., Lourenço, T., Maroco, J., van der Linde, P., & Oliveira, M. M. (2013). Drought stress response in *Jatropha curcas*: Growth and physiology. *Environmental and Experimental Botany*, 85, 76–84.
- Saruhan, N., Terzi, R., Sağlam, A., & Kadioğlu, A. (2010). Scavenging of reactive oxygen species in apoplastic and symplastic areas of rolled leaves in *Ctenanthe setosa* under drought stress. *Acta Biologica Hungarica*, 61(3), 282–298.
- Sárvári, É., Gellén, G., Sági-Kazár, M., Schlosser, G., Solymosi, K., & Solti, Á. (2022). Qualitative and quantitative evaluation of thylakoid complexes separated by Blue Native PAGE. *Plant Methods*, 18(1), 23.
- Sárvári, É., Mihailova, G., Solti, Á., Keresztes, Á., Velitchkova, M., & Georgieva, K. (2014). Comparison of thylakoid structure and organization in sun and shade *Haberlea rhodopensis* populations under desiccation and rehydration. *Journal of Plant Physiology*, 171(17), 1591–1600.
- Shao, R. X., Xin, L. F., Zheng, H. F., Li, L. L., Ran, W. L., Mao, J., & Yang, Q. H. (2016). Changes in chloroplast ultrastructure in leaves of drought-stressed maize inbred lines. *Photosynthetica*, 54(1), 74–80.
- Sipka, G., Magyar, M., Mezzetti, A., Akhtar, P., Zhu, Q., Xiao, Y., Han, G., Santabarbara, S., Shen, J.-R., Lambrev, P. H., & Garab, G. (2021). Light-adapted charge-separated state of photosystem II: Structural and functional dynamics of the closed reaction center. *The Plant Cell*, 33(4), 1286–1302.
- Solymosi, K., Morandi, D., Bóka, K., Böddi, B., & Schoefs, B. (2012). High biological variability of plastids, photosynthetic pigments and pigment forms of leaf primordia in buds. *Planta*, 235(5), 1035–1049.
- Sóti, A., Ounoki, R., Kósa, A., Mysliwa-Kurdziel, B., Sárvári, É., & Solymosi, K. (2023). Ionic, not the osmotic component, is responsible for the salinity-induced inhibition of greening in etiolated wheat (*Triticum aestivum* L. cv. Mv Béres) leaves: A comparative study. *Planta*, 258(5), 102.
- Strasser, R. J., Srivastava, A., & Tsimilli-Michael, M. (2000). The fluorescence transient as a tool to characterize and screen photosynthetic samples. In M. Yunus, U. Pathre, & P. Mohanty (Eds.), *Probing Photosynthesis: Mechanism, Regulation & Adaptation* (1st Edition, Vol. 25, pp. 445–483). CRC Press.
- Terzi, R., Guler, N., Çalişkan, N., & Kadioğlu, A. (2013). Lignification response for rolled leaves of *Ctenanthe setosa* under long-term drought stress. *Turkish Journal of Biology*, 37(5), 614–619.
- Terzi, R., & Kadioglu, A. (2006). Drought stress tolerance and the antioxidant enzyme system in *Ctenanthe setosa*. *Acta Biologica Cracoviensia Series Botanica*, 48(2), 89–96.
- Toldi, O., Tuba, Z., & Scott, P. (2009). Vegetative desiccation tolerance: Is it a goldmine for bioengineering crops? *Plant Science*, 176(2), 187–199.
- Ünnep, R., Nagy, G., Markó, M., & Garab, G. (2014a). Monitoring thylakoid ultrastructural changes in vivo using small-angle neutron scattering. *Plant Physiology and Biochemistry*, 81, 197–207.
- Ünnep, R., Paul, S., Zsiros, O., Kovács, L., Székely, N. K., Steinbach, G., Appavou, M.-S., Porcar, L., Holzwarth, A. R., Garab, G., & Nagy, G. (2020). Thylakoid membrane reorganizations revealed by small-angle neutron scattering of *Monstera deliciosa* leaves associated with non-photochemical quenching. *Open Biology*, 10(9), 200144.
- Ünnep, R., Zsiros, O., Solymosi, K., Kovács, L., Lambrev, P. H., Tóth, T., Schweins, R., Posselt, D., Székely, N. K., Rosta, L., Nagy, G., & Garab, G. (2014b). The ultrastructure and flexibility of thylakoid membranes in leaves and isolated chloroplasts as revealed by small-angle neutron scattering. *Biochimica et Biophysica Acta (BBA) - Bioenergetics*, 1837(9), 1572–1580.
- Yokono, M., Takabayashi, A., Kishimoto, J., Fujita, T., Iwai, M., Murakami, A., Akimoto, S., & Tanaka, A. (2019). The PSI–PSII mega-complex in green plants. *Plant and Cell Physiology*, 60(5), 1098–1108.
- Zampirolo, J. B., Pinheiro, C. L., Santos, V. F. dos, Braga, P. C. S., Martins, J. P. R., Silva, D. M., & Falqueto, A. R. (2021). Analyses of OJIP transients in leaves of two epiphytic orchids under drought stress. *Ornamental Horticulture*, 27, 556–565.
- Zhang, F. J., Zhang, K. K., Du, C. Z., Li, J., Xing, Y. X., Yang, L. T., & Li, Y. R. (2015). Effect of drought stress on anatomical structure and chloroplast ultrastructure in leaves of sugarcane. *Sugar Tech*, 17(1), 41–48.
- Zlatev, Z., & Lidon, F. C. (2012). An overview on drought induced changes in plant growth, water relations and photosynthesis. *Emirates Journal of Food and Agriculture*, 57–72.

SUPPORTING INFORMATION

Additional supporting information can be found online in the Supporting Information section at the end of this article.

How to cite this article: Hembrom, R., Ünnep, R., Sárvári, É., Nagy, G. & Solymosi, K. (2025) Dynamic *in vivo* monitoring of granum structural changes of *Ctenanthe setosa* (Roscoe) Eichler during drought stress and subsequent recovery. *Physiologia Plantarum*, 177(1), e14621. Available from: <https://doi.org/10.1111/ppl.14621>

Supporting Information

Article title: Dynamic *in vivo* monitoring of granum structural changes of *Ctenanthe setosa* (Roscoe) Eichler during drought stress and subsequent recovery

Authors: Richard Hembrom¹, Renáta Ünnepe², Éva Sárvári³, Gergely Nagy⁴, Katalin Solymosi¹

¹Department of Plant Anatomy, ELTE Eötvös Loránd University, Hungary

²Neutron Spectroscopy Department, HUN-REN Centre for Energy Research, Budapest, Hungary

³Department of Plant Physiology and Molecular Plant Biology, ELTE Eötvös Loránd University, Hungary

⁴Neutron Scattering Division, Oak Ridge National Laboratory, Oak Ridge, Tennessee 37831, USA

The following Supporting Information is available for this article:

Figure S1 Fitting accuracy of the small-angle neutron scattering curve.

Figure S2 Small-angle neutron scattering (SANS) sample setup at the “Yellow Submarine” instrument in the Budapest Neutron Center.

Figure S3 Soil relative water content changes during the experiments.

Figure S4 Complex and polypeptide patterns of thylakoids isolated from leaves of control *C. setosa* plants.

Figure S5 Changes in the thylakoid organization of the leaves of differently treated *C. setosa*.

Figure S6 Kinetics of rewatering-induced swelling of the grana in the leaves of a 45- and 48-days drought-stressed *C. setosa* plant in case of ‘Dry 5’ and ‘Dry 6’ plants, respectively.

Table S1 Summary of the features of the parameters (F_M , V_J , V_I and Φ_{i_Pav}) associated with chlorophyll fluorescence obtained from the fast chlorophyll fluorescence kinetic (OJIP) curves of

the leaves of differently treated *C. setosa* leaves.

Table S2 Repeat distance (RD) values of the grana in various leaves of control (Ctrl) *C. setosa* plants.

Table S3 Repeat distance (RD) values of the grana in various leaves of 41-days drought-stressed (Dry) *C. setosa* plants.

Methods S1. Small-angle neutron scattering (SANS) experiments at the Budapest Neutron Center.

Methods S2. The mean of the skewed normal distribution and the error propagation for the SANS measurement at Oak Ridge National Laboratory.

Figure S1 Small-angle neutron scattering curve (blue) from a dry *C. setosa* leaf (blue line), fitted with the combination of multiple power functions, Gaussian peaks, and a skewed normal distribution (centered around c.a. 0.33 nm^{-1}) (orange curve).

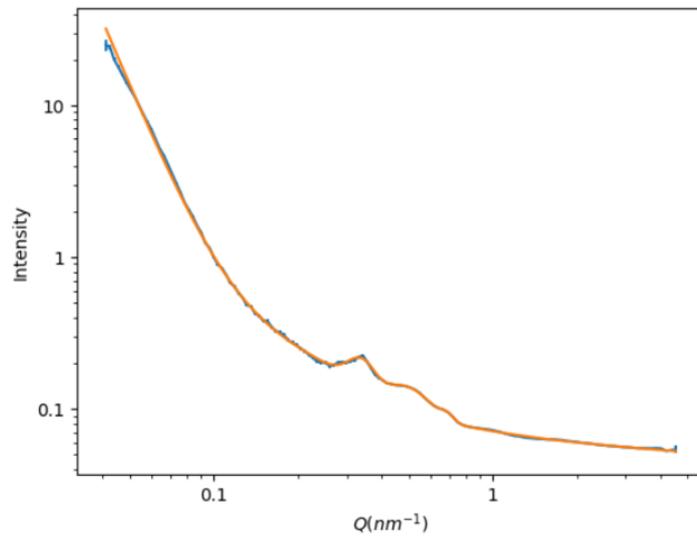


Figure S2 Small-angle neutron scattering (SANS) sample setup at the “Yellow Submarine” instrument in the Budapest Neutron Center. Two leaves were fixed to the end of the collimation section.



Figure S3 Representative soil relative water content changes of a control (well-watered) and a drought-stressed *C. setosa* plant subjected to water withdrawal for 45 days (background color: peach) followed by 1 day (light blue), 7 days (salmon) and 21 days (light green) of re-watering period (the beginning of rewatering is indicated by an arrow).

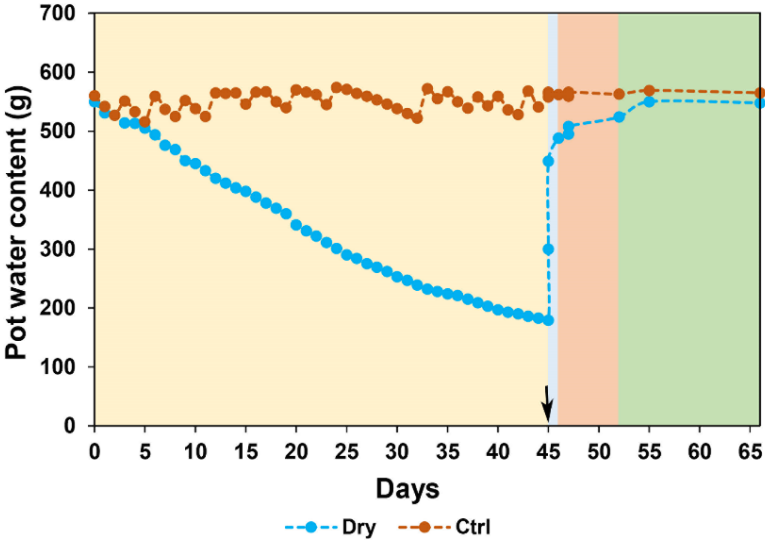


Figure S4 Complex and polypeptide patterns of thylakoids isolated from leaves of control *C. setosa* plants. Thylakoids ($500 \mu\text{g Chl ml}^{-1}$) were solubilized using 1% β -DM plus 1% digitonin and separated in 4.3-12% BN gel gradient followed by SDS PAGE. Some polypeptide spots determining the identity of the complexes unequivocally could be recognized as in Basa et al (2014). Standard proteins (St, kDa): PAGE Ruler Plus Prestained Protein Ladder (Thermo Scientific 26619, lot: 00813689). LHC – light-harvesting complex, LHCII-a – LHCII-assembly: CP29-CP24-LHCII-t, PSII-m2 – CS, PSII-m1, a little larger complex than PSII-m also containing PSII proteins, Cyt *b₆/f* – cytochrome *b₆/f* complex, s – supercomplex, t-trimer, d – dimer, m – monomer. Some remained complexes containing chlorophyll (PSI-subcomplexes, LHCII-t) and polypeptides used for identification of complexes are shown on the 2.D parts of the figure.

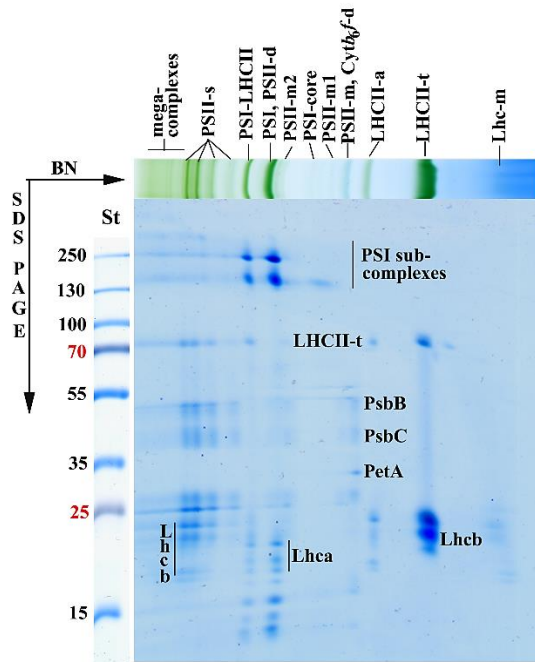


Figure S6 Kinetics of rewatering-induced swelling of the grana in the leaves of a 45- and 48-days drought-stressed *C. setosa* plant in case of 'Dry 5' and 'Dry 6' plants, respectively. The error-bars are derived from the error of the peak position of Gaussian in the fitting results. Measurements were performed at "Yellow Submarine", Budapest Neutron Center.

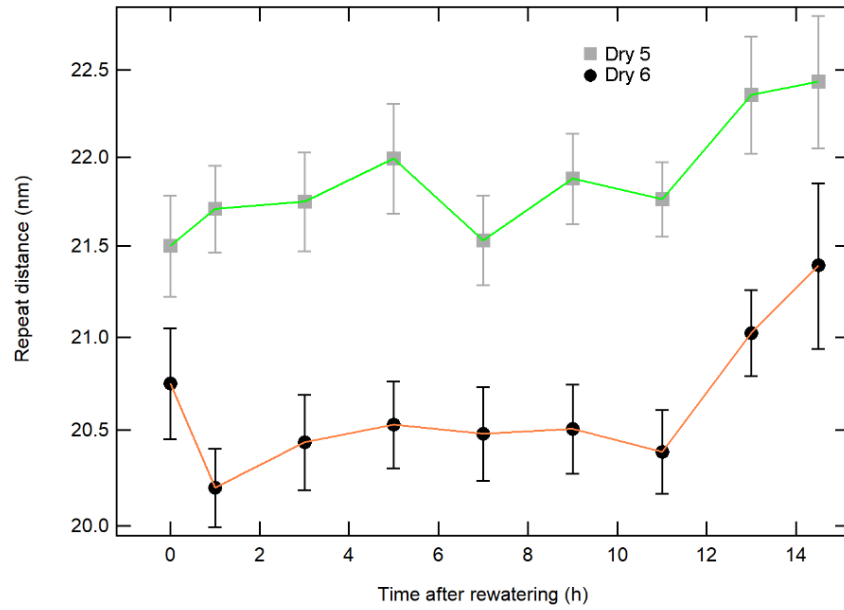


Table S1 Summary of the features of the parameters (F_M , V_J , V_I and Φ_{Pav}) associated with chlorophyll fluorescence obtained from the fast chlorophyll fluorescence kinetic (OJIP) curves of the leaves of differently treated *C. setosa* leaves. Control ('Ctrl'), 40-49 days drought-stressed ('Dry'), and subsequently recovered *C. setosa* plants ('R-1d', 'R-7d' and 'R-21d' were sampled 1 day, 7 days and 21 days after rewatering, respectively). Averaged values with the standard errors are depicted where $n=9-20$. Different letters indicate statistically significant differences across the samples according to Kruskal-Wallis non-parametric ANOVA followed by Dunn's multiple comparisons post hoc test ($P < 0.05$).

	F_M	V_J	V_I	Φ_{Pav}
Ctrl (n=18)	32272 ± 385 ^a	0.41 ± 0.00 ^a	0.85 ± 0.00 ^{ab}	963.20 ± 1.59 ^a
Dry (n=20)	37502 ± 333 ^b	0.47 ± 0.00 ^b	0.87 ± 0.00 ^c	960.10 ± 1.00 ^{ac}
R-1d (n=19)	36275 ± 279 ^b	0.46 ± 0.00 ^b	0.87 ± 0.00 ^{acd}	955.60 ± 1.03 ^{bc}
R-7d (n=9)	36593 ± 484 ^b	0.48 ± 0.00 ^b	0.85 ± 0.00 ^b	954.80 ± 1.03 ^{bc}
R-21d (n=18)	33107 ± 301 ^a	0.43 ± 0.01 ^a	0.84 ± 0.01 ^{bd}	945.60 ± 1.61 ^d

Table S2 Repeat distance (RD) values of the grana in various leaves of control (Ctrl) *C. setosa* plants. SANS curves represent statistically averaged information over the entire sample volume in the neutron beam. RD values are calculated from the fitting results of the SANS curves. Error-bars are derived via error propagation from the error of the mean of the fitted skewed normal distribution. The numbers after 'Ctrl' as well as after 'leaf' refer to given plants and their specific leaves.

Plant	Repeat distance (nm)
Ctrl 1, leaf 1	20.44 ± 0.02
Ctrl 1, leaf 2	20.90 ± 0.04
Ctrl 1, leaf 3	20.83 ± 0.03
Ctrl 2, leaf 1	20.22 ± 0.04
Ctrl 2, leaf 2	20.40 ± 0.02
Ctrl 2, leaf 3	20.16 ± 0.03
Ctrl 3, leaf 1	20.39 ± 0.02
Ctrl 3, leaf 2	20.73 ± 0.02
Ctrl 3, leaf 3	20.56 ± 0.02

Table S3 Repeat distance (RD) values of the grana in various leaves of 41-days drought-stressed (Dry) *C. setosa* plants. SANS curves represent statistically averaged information over the entire sample volume in the neutron beam. RD values are calculated from the fitting results of the SANS curves. Error-bars are derived via error propagation from the error of the mean of the fitted skewed normal distribution. The numbers after ‘Dry’ as well as after ‘leaf’ refer to given plants and their specific leaves. Leaves with flat or rolled leaf blades were measured (‘flattened’ and ‘rolled’, respectively). Positions A and B refer to different measured regions of the same leaf.

Measured leaf area	Repeat distance (nm)
Dry 1, leaf 1, flattened	19.85 ± 0.06
Dry 1, leaf 1, rolled	19.82 ± 0.02
Dry 1, leaf 2	20.08 ± 0.04
Dry 1, leaf 3	20.17 ± 0.03
Dry 2, leaf 1	19.59 ± 0.05
Dry 2, leaf 2	20.03 ± 0.02
Dry 2, leaf 3	19.49 ± 0.02
Dry 3, leaf 1	18.75 ± 0.04
Dry 3, leaf 2	18.95 ± 0.05
Dry 3, leaf 3	18.66 ± 0.30
Dry 4, leaf 1, position A	18.08 ± 0.02
Dry 4, leaf 1, position B	18.12 ± 0.08
Dry 4, leaf 2	18.87 ± 0.37
Dry 4, leaf 3	20.43 ± 1.11
Dry 4, leaf 4	18.36 ± 0.03

Methods S1. Small-angle neutron scattering (SANS) experiments at the Budapest Neutron Center SANS measurements were carried out at the “Yellow Submarine” SANS instrument of the Budapest Neutron Center (BNC, Budapest, Hungary). The sample-to-detector distance, the collimation distance, and the wavelength were set to 5.37 m (Plant 5), 5.3 m (Plant 6), 4.5 m and 0.613 nm, respectively. Intact rooted plants in pots filled with soil were placed on a table. Two leaves were fixed to the end of the collimation section of the beamline (Fig S2). The raw data were treated with the BerSANS program (Keiderling, 2002). The RD values were obtained by fitting a linear combination of a constant, a power and a Gauss function around the Bragg peak. Further details can be found in our previous work (Ünnep et al., 2014).

Methods S2. The mean of the skewed normal distribution can be calculated from the parameters q_{c2} and sk_2 parameters, and w_2 which relates to the width of the distribution.

$$q_{c2_mean} = q_{c2} + \frac{w_2}{2} \sqrt{\frac{2}{\pi}} \frac{sk_2}{\sqrt{1 + sk_2^2}}$$

The error bar assigned to the mean was calculated from the standard deviation of the 3 fitting parameters through the equation:

$$dq_{c2_mean} = \sqrt{dq_{c2}^2 + dw_2^2 \left(\frac{1}{2} \sqrt{\frac{2}{\pi}} \frac{sk_2}{\sqrt{1 + sk_2^2}} \right)^2 + dsk_2^2 \left(\frac{w_2}{2} \sqrt{\frac{2}{\pi}} \left(\frac{1}{\sqrt{1 + sk_2^2}} - \frac{sk_2^2}{(1 + sk_2^2)^{\frac{3}{2}}} \right) \right)^2}$$

The standard deviation of the calculated RD can be calculated as:

$$dRD = \frac{2\pi dq_{c2_mean}}{q_{c2_mean}^2}$$

References

- Basa, B., Lattanzio, G., Solti, Á., Tóth, B., Abadía, J., Fodor, F., & Sárvári, É. (2014). Changes induced by cadmium stress and iron deficiency in the composition and organization of thylakoid complexes in sugar beet (*Beta vulgaris* L.). *Environmental and Experimental Botany*, *101*, 1–11. <https://doi.org/10.1016/j.envexpbot.2013.12.026>
- Keiderling, U. (2002). The new 'BerSANS-PC' software for reduction and treatment of small angle neutron scattering data. *Applied Physics A*, *74*(1), s1455–s1457. <https://doi.org/10.1007/s003390201561>
- Ünnep, R., Zsiros, O., Solymosi, K., Kovács, L., Lambrev, P. H., Tóth, T., Schweins, R., Posselt, D., Székely, N. K., Rosta, L., Nagy, G., & Garab, G. (2014). The ultrastructure and flexibility of thylakoid membranes in leaves and isolated chloroplasts as revealed by small-angle neutron scattering. *Biochimica et Biophysica Acta (BBA) - Bioenergetics*, *1837*(9), 1572–1580. <https://doi.org/10.1016/j.bbabi.2014.01.017>